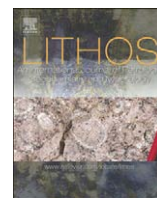




Contents lists available at ScienceDirect

Lithos

journal homepage: [www.elsevier.com/locate/lithos](http://www.elsevier.com/locate/lithos)

## Peralkaline granitoid magmatism in the Mongolian–Transbaikalian Belt: Evolution, petrogenesis and tectonic significance

B.M. Jahn<sup>a,\*</sup>, B.A. Litvinovsky<sup>b</sup>, A.N. Zanzilevich<sup>b</sup>, M. Reichow<sup>c</sup>

<sup>a</sup> Institute of Earth Sciences, Academia Sinica, Nangang, Taipei 11529, Taiwan

<sup>b</sup> Dept. of Geological and Environmental Sciences, Ben Gurion University of the Negev, Beer Sheva 84105, Israel

<sup>c</sup> Dept. of Geology, University of Leicester, University Road, Leicester LE1 7RH, UK

### ARTICLE INFO

#### Article history:

Received 8 January 2009

Received in revised form 22 May 2009

Accepted 4 June 2009

Available online xxx

#### Keywords:

Peralkaline granite

Syenite

Sr–Nd isotopes

Petrogenesis

CAOB (Central Asian Orogenic Belt)

Mongolia and Transbaikalia

Juvenile continental crust

### ABSTRACT

The Central Asian Orogenic Belt (CAOB) is well-known for its massive generation of juvenile crust in the Phanerozoic. In eastern CAOB, voluminous peralkaline and alkaline (alkali-feldspar) granitoids and genetically related bimodal volcanics were emplaced in three stages from Early Permian to late Mesozoic: 295–270 Ma, 230–190 Ma and 150–120 Ma. They occur as huge granitoid belts in extensional tectonic settings and form a complex network of about 12 million km<sup>2</sup> in area. Among them the 2500 km-long Mongolian–Transbaikalian Belt (MTB) is the most spectacular and it comprises more than 350 granite–syenite plutons and stocks, with numerous co-genetic volcanic fields. The three stages of granitoids have similar chemical compositions but show temporal variation in Nd isotopic composition. Initial  $\epsilon\text{Nd}(T)$  values range from  $-1$  to  $-5$  for the Early Permian,  $0$  to  $+4$  for the early Mesozoic, and  $-2$  to  $-3.5$  for the late Mesozoic granitoids. The negative  $\epsilon\text{Nd}(T)$  values observed in the MTB are not typical of the CAOB granitoids, which are generally characterized by positive values. However, several pieces of evidence suggest that the MTB peralkaline and alkali feldspar granitoids were produced from enriched mantle-derived sources. The evidence includes: (1) Felsic and mafic rocks formed in the same stage have similar initial Nd–Sr isotopic ratios and Sm–Nd model ages ( $T_{\text{DM}}$ ). (2) The granitoid belts extend over thousands of kilometers and intersect distinct crustal provinces, but no correlation is found in chemical compositions between the granitoids and country rocks. (3) The abundant syenites are considered to be cogenetic or, in some cases, parental to the granites. Experimental and isotope data argue for the derivation of syenites from an enriched mantle source, thus the granites (and comendites) are regarded as mantle-derived. (4) A study of melt inclusions in quartz phenocrysts of comendite indicates a high liquidus temperature of 1000–1100 °C for the magma generation. This suggests that the silicic magma was generated in an unusually high temperature condition which is likely produced by basaltic magma that underplated the lower crust. The generation of voluminous peralkaline and alkaline (alkali-feldspar) granitoids and genetically related bimodal volcanic rocks represents an important addition of juvenile crustal mass to the Earth's continental crust during a time span of about 150 Ma from Late Paleozoic to Late Mesozoic.

© 2009 Elsevier B.V. All rights reserved.

### 1. Introduction

Since “A-type granite” was first recognized about 30 years ago (Loiselle and Wones, 1979; Collins et al., 1982), a spectrum of alkali-rich granitic rocks has been included in this type, and their compositions range from syenogranite through peralkaline granite, syenite, rapakivi granite, charnockite, and finally to fluorine-rich topaz granite (e.g., Collins et al., 1982; Whalen et al., 1987; Eby, 1992; Patiño Douce, 1997; Wu et al., 2002; Bonin, 2007). Such a wide range of

composition leads to constant debate about the origin of A-type granites (e.g., Whalen et al., 1987; Bonin, 2004; Whalen, 2005; Bonin, 2007). Clearly, a unified model for the generation of A-type granitoids is unrealistic.

In this paper, we study the origin of peralkaline and alkaline (particularly, alkali-feldspar) granites and their extrusive equivalents from Transbaikalia of eastern Siberia (Russia). The term ‘peralkaline granitoids’ is used for granite and syenite with apatitic index  $\text{NK}/\text{A} > 1$ , containing Na-rich amphibole and pyroxene. The ‘alkali-feldspar granitoids’ include granite and syenite with  $\text{NK}/\text{A}$  ranging from 0.9 to 1, and alumina saturation index  $\text{A}/\text{CNK} = 1 \pm 0.15$ ; they consist mainly of perthitic alkali feldspar, quartz, Fe-rich biotite, Ca–Na amphibole (the latter mostly in syenite). In the paper we use abbreviations PA and AFS for peralkaline and alkali-feldspar granitoids,

\* Corresponding author. Institute of Earth Sciences, Academia Sinica, P.O. Box 1-55, Nangang, Taipei, 11529, Taiwan. Tel.: +886 2 2783 9910x103; fax: +886 2 2788 3493. E-mail address: [jahn@earth.sinica.edu.tw](mailto:jahn@earth.sinica.edu.tw) (B.M. Jahn).

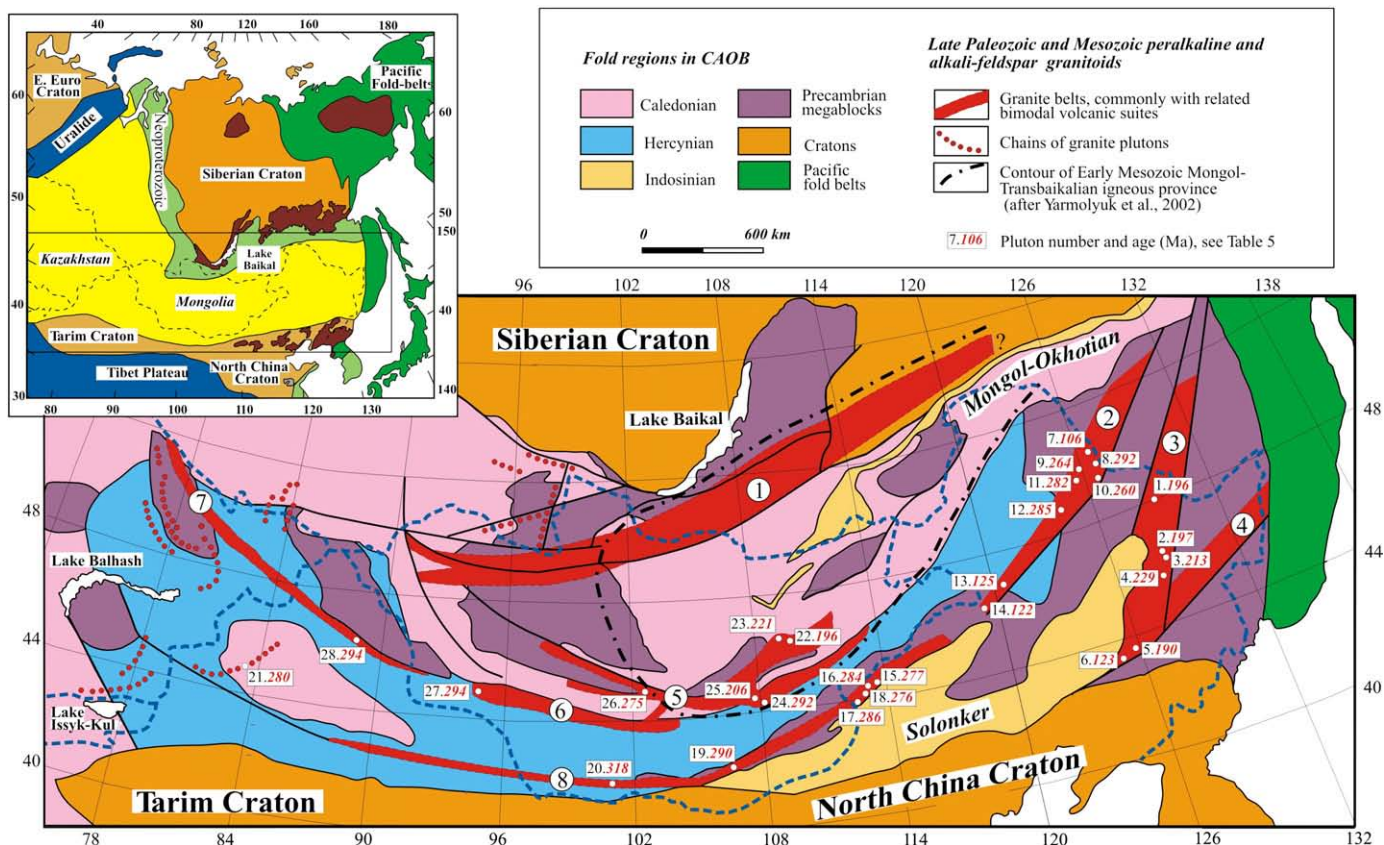


**Fig. 1.** Distribution of the Late Paleozoic and Mesozoic granitoid belts in the Central Asian Orogenic Belt. The map area corresponds to the rectangle of the inset map. The numbers of plutons correspond to that in Table 5; ages (Ma, in red) beside numbers are also taken from this table. Granite belts: 1 = Mongolian–Transbaikalian, 2 = Great Xing’an, 3 = Zhangguangcai, 4 = Jiamusi, 5 = Gobi–Altai, 6 = Main Mongolian Lineament, 7 = Eastern Kazakhstan, 8 = Gobi–Tien Shan. Data sources: Leontiev et al., 1981; Yarmolyuk, 1983; Zanzivich et al., 1985; Geological map of Mongolia (1: 1,500,000), 1989. The map of magmatic rocks of Transbaikalia, Eastern Sayan and the adjacent areas in Mongolia (1: 1,500,000) was produced using the following literature data: Han et al. (1997), Wang S. et al. (1995), Hong D.W. et al. (1994, 1996), Yarmolyuk et al. (2001, 2002, 2005), Wu et al. (2002), Jahn (2004), Kovalenko et al. (2004), and Yanshin (1980).

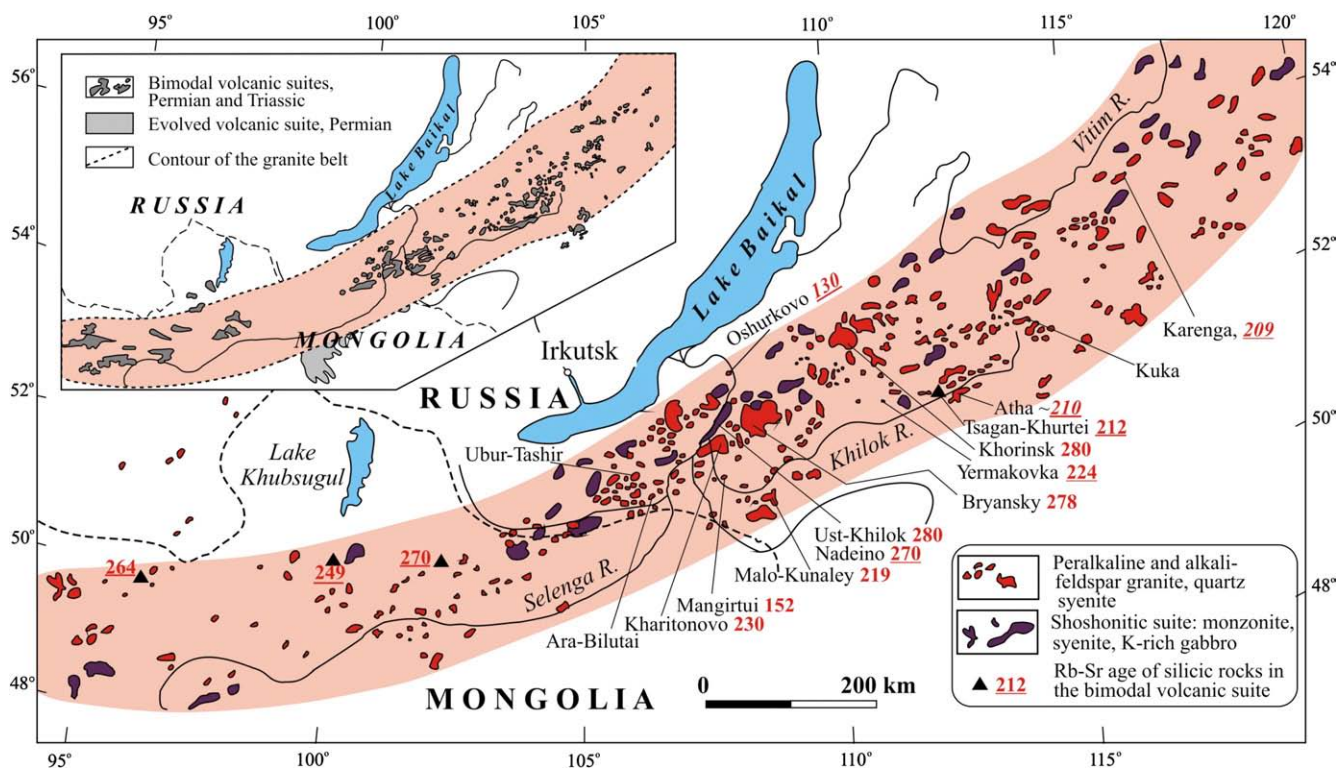


**Fig. 2.** Distribution of the Late Paleozoic and Mesozoic PA and AFS granitoids in the Mongolian–Transbaikalian Belt. The numbers by the pluton names designate the U–Pb (zircon) and Rb–Sr (WR, underlined) isotopic ages (in Ma). In the western part of the belt, Rb–Sr ages of trachyrhyolite and pantellerite from the bimodal volcanic suites in three localities are shown (after Yarmolyuk et al., 2005; see Table 1). In the inset, the main bimodal volcanic fields are also shown (the smaller fields are shown off scale).

Please cite this article as: Jahn, B.M., et al., Peralkaline granitoid magmatism in the Mongolian–Transbaikalian Belt: Evolution, petrogenesis and tectonic significance, *Lithos* (2009), doi:10.1016/j.lithos.2009.06.015

respectively. The integral term for both groups is 'highly alkaline granitoids'.

Highly alkaline granitoids occur throughout the world, and they are especially widespread in the Central Asian Orogenic Belt (CAOB; Fig. 1). The CAOB, also termed "the Altaid Tectonic Collage", is an immense accretionary orogen (Sengör et al., 1993; Sengör and Natal'in, 1996; Jahn et al., 2000; Kovalenko et al., 2004; Windley et al., 2007). It extends from the Urals eastwards to the Pacific coast, and southwards from the Siberian and Baltica cratons to the Sino-Korean and Tarim cratons (Fig. 1, inset). The crustal evolution of the CAOB began at c. 1.0 Ga (Khain et al., 2002; Kovalenko et al., 2004; Windley et al., 2007) and continued to c. 250 Ma, when the Palaeo-Asian ocean was closed along the Solonker suture (Xiao et al., 2003; Chen and Jahn, 2004; Chen et al., 2009; Wu et al., 2007a). Igneous activity in Central Asia spanned the entire Phanerozoic and continued into the Mesozoic. It resulted in emplacement of abundant juvenile granitoids and volcanic rocks (Kovalenko et al., 1994; Jahn et al., 2000; Kovalenko et al., 2004; Jahn, 2004; Zhang et al., 2008). The voluminous juvenile crust distinguishes the CAOB from other classic Phanerozoic orogenic belts, such as Caledonides and Hercynides in Europe (e.g., Jahn et al., 2000; Jahn, 2004; Wu et al., 2000).

The purpose of this study is to discuss the origin of PA and AFS granitoids using a variety of petrological, geochemical and isotopic data. We focus on the largest Mongolian–Transbaikalian granitoid belt, which is characterized by the occurrence of abundant post-orogenic and within-plate PA and AFS granitoids (belt #1 in Figs. 1 and 2). We conclude that the highly alkaline silicic magmas were emplaced in three stages from late Paleozoic to late Mesozoic. They

were derived from enriched mantle sources with limited role of recycled crustal component, and hence they have contributed substantially to the growth of the Asian continent.

## 2. Geological setting and field occurrence of the granitoids

The great majority of PA and AFS granitoids was produced in the CAOB during Late Paleozoic and Mesozoic (Kovalenko et al., 2004; Yarmolyuk et al., 2001, 2002, 2005). We present in Fig. 1 the distribution of Late Paleozoic and Mesozoic granitoids and coeval volcanic suites within the CAOB. The granitoid plutons and volcanic fields form an extensive network of curvilinear belts. The network is superimposed on a complex collage of Paleozoic ("Caledonian" and "Hercynian") terranes and Precambrian micro-continent (Sengör et al., 1993; Windley et al., 2007). Among the granitic belts, the Mongolian–Transbaikalian Belt (MTB) is the largest and most representative in terms of the lithological assemblage.

The MTB, earlier recognized as the Mongolian–Transbaikalian Rift Province by Zandvilevich et al. (1985), extends from northern Mongolia, Transbaikalia (Russia) and further to the Aldan shield. The MTB runs along the southern border of the Siberian Craton, and crosscuts Precambrian micro-continental blocks (Khangai, Dzhida, Barguzin) along the Dzhida suture in its western part (Kovalenko et al., 2004). The MTB covers a distance of >2500 km, and varies in width from 150 to 250 km (Fig. 1). The northeastern boundary of the belt is currently unknown.

The central part of the MTB is situated in Transbaikalia, and has been mapped at a scale of 1:50,000 since 1950's. The mapping has delineated numerous plutons made up of PA and AFS granitoids (Fig. 2). In northern

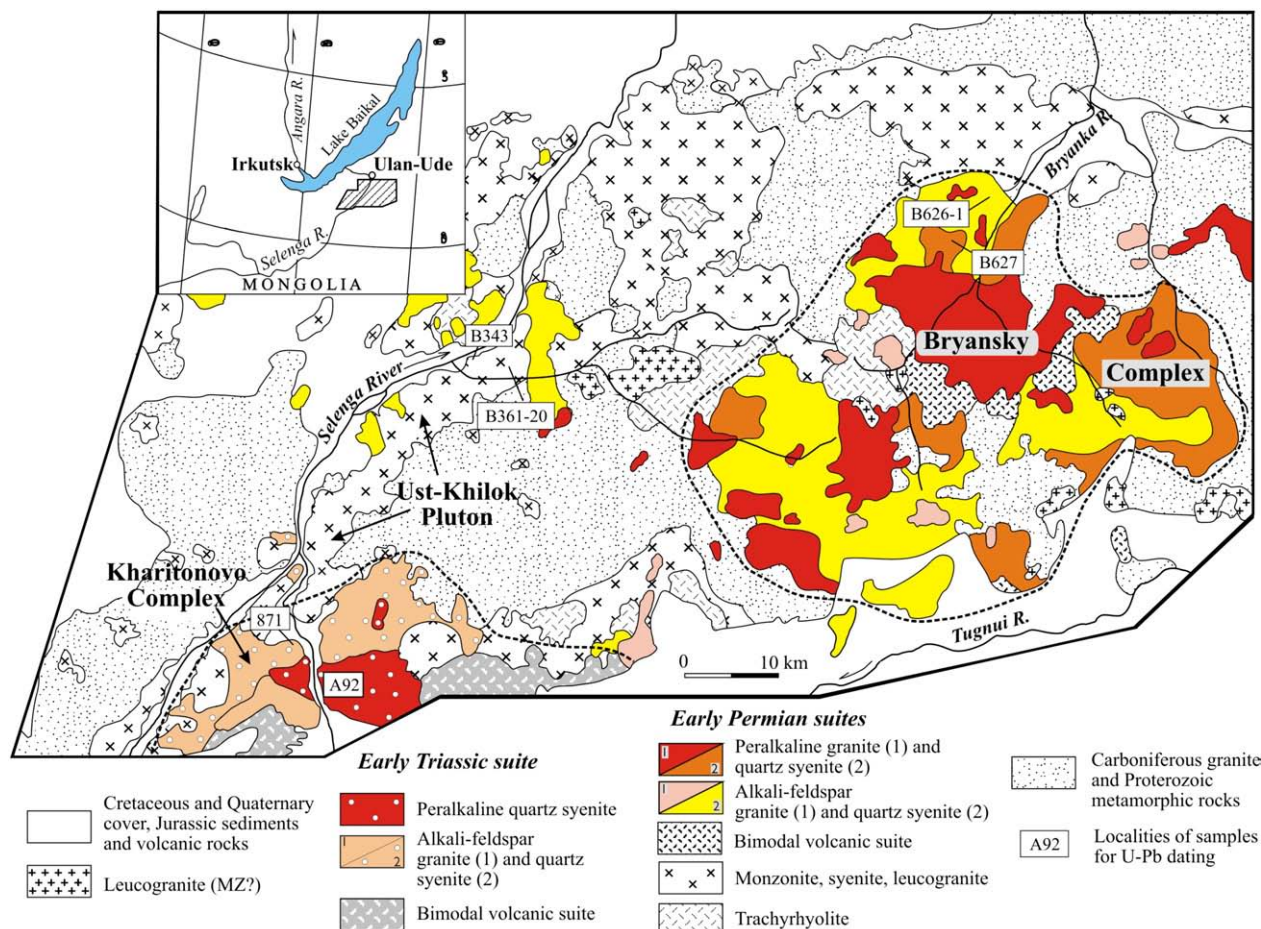


Fig. 3. Simplified geological map of the area between the Selenga, Uda and Tugnui Rivers in Transbaikalia, Russia. The map illustrates the close association of the Late Permian and Late Triassic AFS–PA granitoids (Bryansky and Kharitonovo complexes) and the Early Permian Ust-Khilok pluton made up of shoshonitic series.

Mongolia such rock types occur widely but are less voluminous. At present, more than 350 plutons are known in the MTB (Zanvilevich et al., 1985, 1995; Wickham et al., 1995). They range in size from 10–15 km<sup>2</sup> to 200 km<sup>2</sup>, with a few large plutons up to 1600 km<sup>2</sup> (Litvinovsky et al., 2002a). The total area occupied by the exposed plutons is more than 9000 km<sup>2</sup> in Transbaikalia only (Litvinovsky et al., 1999).

Generally, the plutonic rocks of the MTB are closely associated in space and time with bimodal volcanic series (K-rich basalt, rhyolite, comendite, and subordinate trachyte) and bimodal dyke swarms. The main volcanic fields are shown in the inset of Fig. 2, and their distribution is equally widespread as the plutonic rocks. All these rocks are confined to a system of SW–NE grabens, forming the Mongolian–Transbaikalian Rift Zone (Zanvilevich et al., 1985; Yarmolyuk et al., 2001). In places, the volcanic sequence exceeds a thickness of 2000 m. Peralkaline and alkali-feldspar granitoids were emplaced into volcanic roofs, suggesting shallow depths of crystallization. Commonly, the sizes of associated intrusive bodies and volcanic fields are in inverse proportion. It could be understood that large plutons probably result from a greater extent of erosion of volcanic cover in the volcanic–plutonic structures. It is likely that the volume of related volcanic rocks was comparable with that of granites and syenites.

The order of emplacement generally starts from AFS syenite, followed by granite to peralkaline syenite (nordmarkite), and finally PA granite. The intrusions of syenite and granite magmas occurred in several successive phases; and the proportion of quartz in syenites increased from 3–6 vol.% in the earlier to 10–15 vol.% in the latest phases. The structure of plutonic bodies depends on their size. As a rule, large plutons are made up of PA and AFS granitoids in variable proportion (e.g. Fig. 3, Bryansky and Kharitonovo Complexes), whereas smaller plutons, with areas <100 km<sup>2</sup>, comprise one or two rock types. Coeval mafic rocks are rare in the granitoid suites under consideration, but they occur as microgranular mafic enclaves and as members of composite dikes in the AFS syenites and PA granite of the Khorinsk and Kharitonovo Complexes (Zanvilevich et al., 1995). In

addition, trachybasalt is abundant in the bimodal volcanic series (Yarmolyuk et al., 2001; Litvinovsky et al., 2001, 2002a).

Apart from the predominant Early Permian and Late Triassic syenite–granite suites, some Late Mesozoic highly alkaline silicic rocks also occur. The emplacement of silicic rocks was connected with the formation of the intra-continental Transbaikalian Rift Province (Fig. 4; Yarmolyuk et al., 1998). During the Late Jurassic to Early Cretaceous (170–110 Ma), massive eruption of alkali basalt, tephrite, phonolite, and latite occurred in an extensive system of grabens. This was accompanied by subordinate trachyte and trachyrhyolite eruptions, and emplacement of dykes and subvolcanic comendite, pantellerite, and alkali-feldspar rhyolite. The Early Cretaceous AFS syenite and quartz syenite are the only coeval silica-saturated plutonic rocks. In fact, their emplacement represents the final stage of formation of the plutonic complex consisting mainly of alkaline monzodiorite and monzonite (Litvinovsky et al., 2002b).

The Late Mesozoic grabens were formed in parallel with the development of metamorphic core complexes which are abundant in southern Transbaikalia and Mongolia (Sklyarov et al., 1994; Donskaya et al., 2008). In some metamorphic core complexes, gneissic PA granite plutons occur, but their volume can only be determined by detailed mapping. In the Zagan metamorphic core complexes, half a dozen small (2–5 km<sup>2</sup>) PA granite stocks or buttes were mapped. The strike and dip of the gneissosity in granite are conformable with that of the surrounding metamorphic rocks, even though the intrusive contact is conspicuous (Zanvilevich et al., 1985). This is best exemplified by the Mangirtui pluton (Fig. 4; Number 2).

The available U–Pb and Rb–Sr age data for PA and AFS granitoids and coeval volcanic suites of the MTB are summarized in Table 1. We note that the Rb–Sr dates generally agree with the U–Pb ages, but the latter show a better precision. The age data reveal three main stages of emplacement of the highly alkaline granitoids: Early Permian (285–270 Ma), Late Triassic (230–210 Ma), and Late Jurassic–Early Cretaceous (~150 Ma and 130–120 Ma). The intrusions of PA and AFS granitoids are

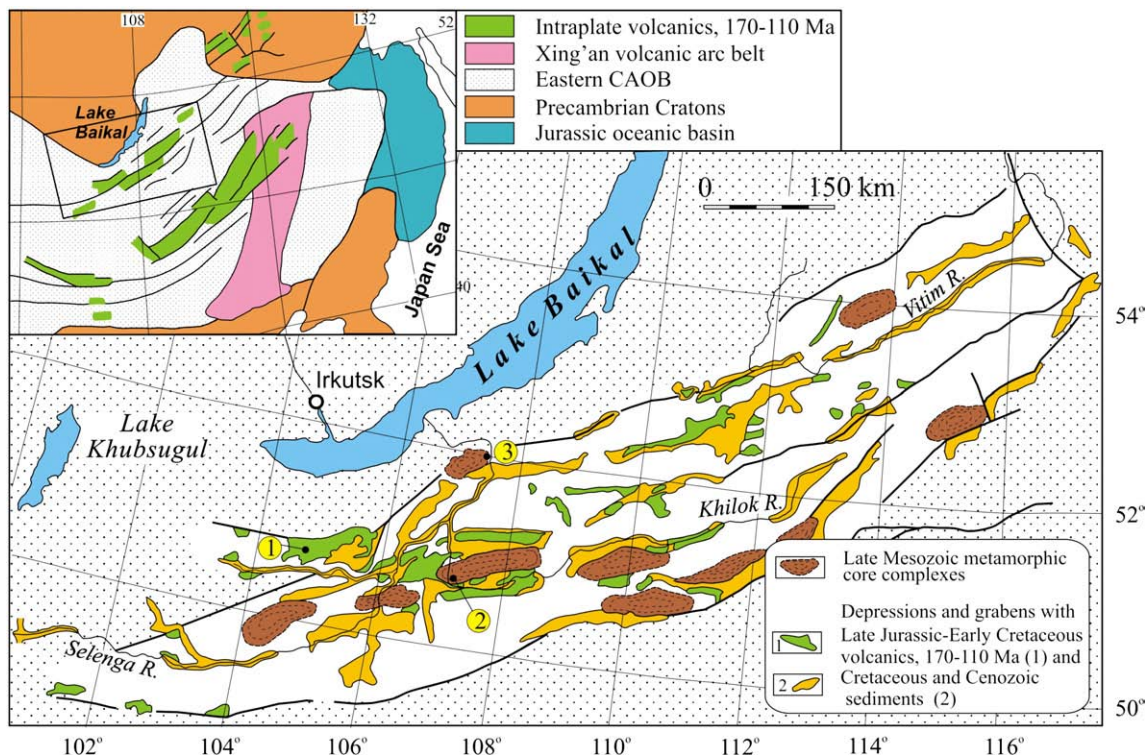


Fig. 4. Schematic map of the Western Transbaikalian Rift Province (after Yarmolyuk et al., 1998, and Donskaya et al., 2008). Numbers in circles: 1, locality of sampled comendite dikes (Tables 2 and 3) in the Malo-Khamardaban volcanic–tectonic structure; 2, the Mangirtui pluton within the Zagan metamorphic core complex; 3, the Oshurkovo pluton. The inset shows the distribution of Late Jurassic–Early Cretaceous (170–110 Ma) volcanic fields (after Yarmolyuk et al., 1998). The area within the box designates the Transbaikalian province.

**Table 1**

Summary of the Rb–Sr and U–Pb geochronological data for highly alkaline igneous suites from the central part of the Mongolian–Transbaikalian Belt.

Rock type	Rb–Sr		U–Pb		
	Age, Ma	( <sup>87</sup> Sr/ <sup>86</sup> Sr) <sub>0</sub>	Sample no.	Rock	Age, Ma
<i>Bryansky Complex</i> <sup>1</sup>					
PA granite	280 ± 6 (n = 20)	0.7053 ± 0.0008	B627	PA syenite	277 ± 1.3
AFS syenite and granites	280 ± 14 (n = 6)	0.7050 ± 0.0010	B626–1	AFS syenite	278 ± 1.6
Comendite, trachyandesite, volcanic rocks	284 ± 4 (n = 5)	0.7062 ± 0.0002			
<i>Khorinsk Complex</i> <sup>2, 10</sup>					
PA syenite and granite	270 ± 15 (n = 5)		M340	PA granite	278 ± 0.9
			M350	PA granite	273 ± 0.4
AFS syenite and granites	268 ± 12 (n = 5)		M347	AFS syenite	279 ± 1.9
Trachyte (bimodal dyke swarm)	288 ± 5 (n = 8)	0.7059 ± 0.0002			
<i>Kharitonovo Complex</i> <sup>3, 10</sup>					
PA syenite and granite	221 ± 1 (n = 18)	0.7064 ± 0.0004	A92	PA syenite	229 ± 0.6
			871	AFS syenite	230 ± 0.7
<i>Malo-Kunalei pluton</i> <sup>10</sup>					
PA quartz syenite			A516	PA granitic pegmatite	219 ± 0.6
<i>Yermakovka pluton</i> <sup>4</sup>					
PA granite	224 ± 1.3 (n = 10)	0.70658 ± 0.0001			
<i>Tsagan–Hurtei volcanic suite</i> <sup>5</sup>					
Comendite, trachybasalt, trachyte	212 ± 5 (n = 13)	0.7046 ± 0.0006			
<i>Karenga pluton</i> <sup>6</sup>					
PA granite	209 ± 5				
<i>Mangirtui pluton</i> <sup>11</sup>					
PA gneissic granite			B611	PA granite	151.6 ± 0.7
<i>Oshurkovo alkali monzonite–syenite Complex</i> <sup>7</sup>					
Monzonite–syenite pegmatite	122 ± 8 (n = 5)	0.7054 ± 1			
<i>Ust–Khilok pluton</i> <sup>8,10</sup>					
Monzonite, syenite	280 ± 18 (n = 9)	0.7060 ± 0.0002	B361–20	syenite	279.5 ± 1.4
			B343	syenite	280.3 ± 1.4
<i>NE Mongolia</i> <sup>9</sup> ; <i>Bimodal volcanic suite</i>					
Trachyrhyolite	270 ± 3				
Trachyrhyolite	264 ± 3				
Pantellerite	249 ± 5				

References: <sup>1</sup> Litvinovsky et al., 2002a; <sup>2</sup> Posokhov et al., 2005; <sup>3</sup> Litvinovsky et al., 1995a,b; <sup>4</sup> Lykhin et al., 2001; <sup>5</sup> Litvinovsky et al., 2001; <sup>6</sup> Stupak, 1999; <sup>7</sup> Litvinovsky et al., 2002b; <sup>8</sup> Litvinovsky et al., 1999; <sup>9</sup> Yarmolyuk et al., 2005; <sup>10</sup> Reichow et al., 2003; <sup>11</sup> Donskaya et al., 2008.

Abbreviations: PA, peralkaline; AFS, alkali-feldspar.

contemporaneous. The age of shoshonitic gabbro–monzonite–syenite suite (Fig. 2) is similar to that of the Early Permian PA and AFS granite–syenite suite (280 ± 1.4 Ma), which is represented by the Ust–Khilok pluton of about 700 km<sup>2</sup> in area (Litvinovsky et al., 1995b).

### 3. Analytical methods

#### 3.1. Whole-rock chemical analysis

Major elements were analyzed using a combination of the wet chemical method, atomic absorption spectrometry and titration. Some trace elements (Rb, Sr, Ba, Y, Zr and Nb) were determined by XRF at the Geological Institute, Siberian Division of the Russian Academy of Sciences, Ulan–Ude. Rare earth and other trace elements (Hf, Ta, Th, U, Ga, V, Cu, Pb, Zn, Sc and Cs) were analyzed by the ICP–MS method at the Department of Geological Sciences, National Taiwan University (NTU), Taipei, and at the Institute of Mineralogy and Geochemistry of Rare Elements, Moscow. The analytical uncertainties are about 2% for major elements, 5–10% for most trace elements, and 1–5% for all REE except Lu (about 10%). The analytical procedures at NTU are briefly described below.

Concentrations of trace elements were determined by ICP–MS using an Agilent 7500 s spectrometer. Rock powders were first fused to make glass beads for XRF major element determination. Used glass beads were then powdered and dissolved in HF/HNO<sub>3</sub> (1:1) mixture in capped Savilex beakers for >2 h at ca. 100 °C, followed by evaporation to dryness, refluxing in 7 N HNO<sub>3</sub> for >12 h at ca. 100 °C. and finally, diluting the sample solution by 2% HNO<sub>3</sub>. An internal standard solution of 5 ppb Rh and Bi was added and the spiked solution was diluted with 2% HNO<sub>3</sub> to a sample/solution weight ratio of 1:2000. An internal standard was used for monitoring the signal shift during ICP–MS measurements. The analytical precision for trace elements was <5% (2-sigma). For more details, see Yang et al. (2005).

#### 3.2. Sr and Nd isotope analyses

Sr and Nd isotopic compositions were determined at the Institute of Earth Sciences (IES), Academia Sinica, Taipei. Powdered samples were dissolved in Savilex bombs, following a series of standard procedures until samples were completely dissolved. Isolation of Sr and Nd was achieved using a 2-column technique, Sr fractions were occasionally further purified using a third column. The first column was packed with 2.5 ml cation exchange resin (Bio-Rad AG50W-X8, 100–200 mesh) and was used to collect Sr and REE fractions. The second column used for Sr purification was packed with 1 ml cation exchange resin, identical to the above. The second column used for Nd isolation was packed with 1 ml Ln-B25-A (Eichron) resin, which was covered on top by a thin layer of anion exchange resin (Bio-Rad AG1-X8, 200–400 mesh).

Mass analyses were performed using a 7-collector Finnigan MAT-262 mass spectrometer in dynamic mode. <sup>143</sup>Nd/<sup>144</sup>Nd ratios were normalized against the value of <sup>146</sup>Nd/<sup>144</sup>Nd = 0.7219, whereas <sup>87</sup>Sr/<sup>86</sup>Sr ratios were normalized to <sup>86</sup>Sr/<sup>88</sup>Sr = 0.1194. During the course of analysis, measurements on NBS-987 Sr standard yielded <sup>87</sup>Sr/<sup>86</sup>Sr = 0.710320 ± 0.000036 (n = 50) using the static mode, and = 0.710237 ± 0.000020 (n = 8) using the dynamic mode. All <sup>87</sup>Sr/<sup>86</sup>Sr ratios reported herein have been duly adjusted to NBS-987 = 0.710250. Our measurements on La Jolla Nd standard yielded 0.511864 ± 0.000006 (n = 4), and on JMC Nd standard, 0.511821 ± 0.000016 (n = 6). No further adjustment on Nd isotopic ratios was made.

#### 3.3. Melt inclusion analyses

The detailed analytical procedures were described in Kuzmin et al. (1999) and Litvinovsky et al. (2001); only a brief description is given below. Melt inclusions were analyzed using a heating stage with a silicon-carbide heating element. The precision of temperature measurement is better than +10 °C for the interval of 700–1000 °C. The homogenization temperatures (T<sub>hom</sub>) were measured in groups of small inclusions (≤5 μm), whereas the chemical composition was

**Table 2**  
Chemical composition of representative plutonic and volcanic highly alkaline rocks from the Mongolian–Transbaikalian Belt.

Sample no.	B370	B626	B425	K117-4	B627	B388	A447-4	B382-2	B167-3	B386	M347	3070	M340	M350
Rock	AFS syenite		AFS	PA syenite		PA gran	Comendite		Basalt	Andesite	AFS syen	AFS gran	PA gran	
Early Permian stage														
Bryansky Complex														
Khorinsk Complex														
SiO <sub>2</sub> (%)	62.70	64.6	73.4	63.6	65	72.6	71.8	72.5	49.3	61.9	65.8	72.18	74	68.8
TiO <sub>2</sub>	0.65	0.69	0.14	0.88	0.62	0.3	0.51	0.42	1.34	0.6	0.51	0.3	0.25	0.31
Al <sub>2</sub> O <sub>3</sub>	18.30	17.35	13.6	16	16.8	12	10.9	11	15.8	16.5	17.3	13.99	13	16.2
Fe <sub>2</sub> O <sub>3</sub>	0.87	1.06	0.7	1.36	1.64	2.4	5.09	5.74	4.78	1.84	0.93	0.81	1.11	1.15
FeO	1.90	1.6	1.05	2.29	1.01	1.59			3.72	3.86	1.27	0.75	0.52	0.66
MnO	0.09	0.13	0.05	0.17	0.12	0.11	0.2	0.21	0.12	0.09	0.12	0.05	0.1	0.11
MgO	0.30	0.37	0.1	0.6	0.28	0.23	0.13	0.23	8.32	1.72	0.17	0.14	0.06	0.06
CaO	0.98	0.51	0.12	0.3	0.75	0.15	0.02	0.25	6.7	2.8	0.38	0.56	0.03	0.06
Na <sub>2</sub> O	6.34	5.96	4.7	6.66	6.33	4.76	4.77	4.41	3.7	4.59	5.31	4.61	4.66	6.53
K <sub>2</sub> O	6.83	6.55	5.2	6.58	6.63	4.74	4.57	4.5	2.29	4.14	6.76	5.38	4.95	5.46
P <sub>2</sub> O <sub>5</sub>	0.08	0.09	0.03	0.12	0.04	0.01	0.02	0.01	0.39	0.18	0.1	0.07	0.02	0.06
LOI	1.01	0.97	1.11	1.75	0.81	0.97	1.71	0.83	3.81	1.8	0.69	0.5	1.06	0.47
Total	100.05	99.88	100.2	100.31	100.03	99.86	99.72	100.10	100.27	100.2	99.34	99.34	99.76	99.87
Trace elements (in ppm)														
Rb	97	96	170	82	130	190	260	270	43	100	120	210	220	147
Sr	190	64	47	14	34	5	38	13	810	660	28	46	4	5
Ba	880	160	250	100	80	47	10	24	620	1500	180	195	53	24
Nb	16	12	20	24	38	35	120	84	14	15	25	44	31	26
Ta	1.20		1.3	0.71		2.6	7.4	5.2	0.5	0.97	1.12	3.16	1.54	1.6
Th	5	10	23	4		11	67	51	4	15	16.82	45.18	21.72	13.1
U	2.4		3.8			2.5					3.46	7.39	2.77	2.56
Zr	340	120	190	250	930	470	2200	1550	220	310	970	500	330	465
Hf	10.0		6.2	4.2		18	53	36	4	8.3	20.0	12.5	8.9	1.9
Y	32	30	19	35	64	80	170	130	30	27	42	43	39	49
Ga	15		17	24		21	21	24			22	23.6	22.1	27
La	65		32	50		75	150	90	36	50	74	57	50	46
Ce	140		61	110		160	340	270	74	92	245.4	141.2	95.78	100.5
Pr											17.5	12.8	9.0	11.0
Nd	69		15	42		60	110	67	34	35	63	43	30	39
Sm	11.0		1.9	7.8		10.0	19.0	14.0	6.5	6.6	10.5	7.9	5.1	7.4
Eu	1.80		0.21	1.1		1.01	1.6	1.1	1.6	1.2	0.76	0.45	0.32	0.33
Gd											7.8	6.0	4.2	6.2
Tb	1.30		0.26	0.84		2	4.3	3.1	0.71	0.8	1.27	1.04	0.71	1.11
Dy											6.8	6.2	4.3	6.8
Ho											1.36	1.32	0.94	1.43
Er											4.12	4.30	3.03	4.43
Tm											0.64	0.75	0.50	0.70
Yb	2.80		2	2.3		8.1	16	12	2	2.5	4.38	5.43	3.58	4.72
Lu	0.41		0.32	0.34		1.1	2.5	2	0.29	0.4	0.72	0.83	0.58	0.70
Eu/Eu*	0.52		0.34	0.46		0.28	0.23	0.21	0.81	0.58	0.26	0.20	0.21	0.15
NK/A	0.97	0.97	0.98	1.13	1.05	1.08	1.17	1.10	0.54	0.73	0.93	0.96	1.00	1.03
A/CNK	0.98	1.00	1.01	0.87	0.92	0.92	0.85	0.89	1.08	1.13	1.06	1.01	1.00	0.97
A/NK	1.03	1.03	1.02	0.89	0.96	0.93	0.85	0.91	1.84	1.37	1.08	1.04	1.00	0.97

Eu\* = (Smn\*Gdn)/2 or (Smn\*2/3 + Tbn\*1/3); NK/A = (Na<sub>2</sub>O + K<sub>2</sub>O)/Al<sub>2</sub>O<sub>3</sub>, mol%. Eu\* = (Smn\*Gdn)/2 or (Smn\*2/3 + Tbn\*1/3); NK/A = (Na<sub>2</sub>O + K<sub>2</sub>O)/Al<sub>2</sub>O<sub>3</sub>, mol%. Abbreviations: AFS = alkali feldspar; PA = peralkaline.

determined in larger inclusions (~30 μm), both heated (homogenized) and unheated. The unheated melt inclusions provide better data for the volatile content, particularly H<sub>2</sub>O, in magma, because heating of inclusions ≥ 10 μm in diameter to magmatic temperatures usually caused partial loss of fluids (e.g., Student and Bodnar, 1999; Reyf, 2004 and references therein). Homogenized melt inclusions (artificial glass) were analyzed using a Camebax ion probe at the JIGGM laboratory in Novosibirsk, Russia. The concentration of H<sub>2</sub>O, in the form of hydrogen, was determined on an IMS-4f microanalyser at the Institute of Microelectronics, Yaroslavl, Russia.

#### 4. Analytical results and interpretation

##### 4.1. Chemical compositions of the MTB granitoids

Major and trace element compositions were determined for about 200 samples collected from 12 igneous complexes and plutons (Fig. 2). The full set of analytical data is given in Supplementary data (Tables S1 to S4). In Table 2 chemical compositions of 46 representative samples

are reported. Most of these samples were also subjected to Sm–Nd and Rb–Sr isotope analyses.

Two successive suites of PA and AFS granitoids occurred in two stages: Early Permian and Late Triassic (stages 1 and 2). The mean compositions of the main rock types in the two suites are very similar. The granitoids are highly enriched in alkalis, up to 13 wt.% in syenite and 11 wt.% in granite (Tables 2 and S1–S4; Fig. 5A). The syenites of both PA and AFS suites are silica-oversaturated. The proportion of normative quartz ranges from 3 to 8%; however, in quartz syenite of later intrusive phase the quartz content attains 12–15%. The syenites and granites of both stages have low Sr (≤70 ppm), but are enriched in Zr, Nb, Y and REE (Figs. 5 and 7). Fig. 5 indicates the A-type affinity of the granitoids.

The PA and AFS granitoids of the two stages are best distinguished by the agpaic index NK/A (Table 2). Although both PA and AFS rocks are mildly metaluminous to mildly peraluminous, their NK/A values range from 0.90 to 0.99 in AFS rocks and from 1.01 to 1.10 (very rarely up to 1.17) in PA rocks. Such a distinction in the agpaic index is mainly caused by higher Na<sub>2</sub>O/Al<sub>2</sub>O<sub>3</sub> ratio in PA granitoids. Fig. 6

M-487	M511	B341	B361-20	B111	B-342	B517-3	B440	B444	1/7a	B446-1	A13	716	722	725
Basalt	Rhyolite	Syenite		Monzonite	Gabbro		Comendite		Trachybasalt		PA granite			
Ust-Khilok pluton							Early Mesozoic stage							
							Tsagan-Khurtei structure			Atha pluton				
51.7	75.2	61.20	62	57.4	48.9	48.7	74.5	72	46.93	45.82	74.4	74.16	73.02	72.32
1.47	0.21	1.17	0.68	1.09	1.41	1.52	0.29	0.34	2.69	2.7	0.25	0.23	0.42	0.42
17.4	12.8	17.40	18.3	19.19	17.4	17.8	10.7	10.95	16.19	16.5	11.38	11.08	12.11	12.47
4.37	1.83	2.55	1.79	2.68	6.06	3.19	4.08	6.7	12.48	13	1.1	0.88	2.2	1.77
5.2	0.57	2.44	1.02	2.92	4.38	6.7					3.08	2.56	1.37	1.68
0.16	0.02	0.11	0.09	0.12	0.18	0.14	0.06	0.15	0.17	0.15	0.1	0.1	0.13	0.12
3.81	0.2	1.07	0.5	1.65	4.34	5.3	0.23	0.2	6.37	6.45	0.14	0.13	0.23	0.3
8.34	0.2	2.00	1.45	3.36	8.94	7.9	0.4	0.2	8.12	8.02	0.2	0.21	0.26	0.31
4.6	4.25	5.34	5.7	4.45	3.81	3.76	3.22	5.03	4.02	4.23	4.29	4.74	4.98	5.12
1.86	4.23	5.67	7.68	5.47	2.01	2.01	5.95	4.17	1.1	0.29	4.44	4.53	4.68	4.94
0.36	0.04	0.26	0.14	0.42	0.51	0.82	0.04	0.05	1.02	1.05	0.02	0.02	0.02	0.03
1.08	0.36	0.37	0.61	0.66	1.88	2.3	0.64	0.59	0.9	2.05	0.54	0.76	0.57	0.5
100.35	99.91	99.58	99.96	99.41	99.82	100.14	100.11	100.38	99.99	100.26	99.94	99.4	99.99	99.98
<i>Trace elements (in ppm)</i>														
98	200	105	120	62	62	29	207	135	10	11	162	133	133	133
692	16	380	260	1225	1260	1500	21	18	1188	1136	6	3	13	7
484	100	1300	800	4140	800	1100	62	110	596	490	56	46	44	53
10	42	27	9	7	6	11	42	55	11	10	54	40	37	32
0.65	3.34		0.55		0.31	0.46					3.29	3.56	2.38	2.1
4.08	45.12		4.81		2.5	2	21	17	2.1		14.99	15	14	17
1.05	9.9		2.29		190						3.78			
249	520	620	680	56	120	190	1024	1450	228	210	990	910	820	725
5.3	21.2		9.5		2.7	4	14	50	5.6		23.4	20.6	20.7	16.7
32.09	54	37	16	21	36	29	52	110	30	22	70	63	52	46
20.2	34		18.4								27	27	25	26
42	90	80	38	41	50	35	91		40	47	19	75	68	81
66.54	189	150	69.38	82	120	77	180		94	100	82	155	168	154
7.7	20.1		7.9						11.4	12.1	4.4	17.0	17.5	18.2
32	72	54	30	36	57	36	72		54.6	56	15	58	65	65
6.4	14.2	9.8	5.2	5.7	8.7	7.3	12.0		10.4	11.1	3.5	10.5	12.5	11.3
1.65	0.72	1.8	1.5	3	2	2	1.5		3.36	3.44	0.32	0.42	1.52	1.42
5.9	12.3		4.3						8.3	9.2	4.4	9.5	10.7	10.1
0.94	2.17	1.3	0.69	0.68	1.3	0.93	1.8		1.26	1.44	1.22	1.64	1.93	1.75
5.3	12.7		3.3						6.4	7.7	9.8	10.8	11.1	9.2
1.07	2.66		0.65						1.27	1.54	2.36	2.5	2.29	2.02
3	8.13		1.77						3.08	3.86	7.64	7.94	7.24	5.8
0.43	1.28		0.28						0.48	0.63	1.31	1.34	1.12	0.91
2.74	8.56	3.40	1.77	1.1	2.7	2	6.1		2.85	3.89	9.14	8.2	7.49	5.65
0.41	1.31	0.50	0.29	0.17	0.38	0.34	0.95		0.41	0.54	1.44	1.4	1.16	0.91
0.82	0.17	0.57	0.97	1.67	0.7	0.86	0.38		1.11	1.04	0.25	0.13	0.4	0.41
0.55	0.90	0.86	0.97	0.69	0.49	0.47	1.10	1.17	0.48	0.44	1.04	1.15	1.09	1.10
1.01	1.09	1.04	0.96	1.18	1.05	1.15	0.88	0.84	1.07	1.13	0.94	0.86	0.90	0.89
1.82	1.11	1.17	1.03	1.45	2.06	2.13	0.91	0.86	2.07	2.27	0.96	0.87	0.91	0.91

shows that PA granites and syenites are richer in Na<sub>2</sub>O than AFS rock types with the same alumina content, both in the Early Permian and Late Triassic suites; higher Na content could provide its excess with respect to alkali feldspars and hence favors crystallization of Na-rich mafic minerals.

In brief, we emphasize that despite a large time span (40–50 Ma) between the two main highly alkaline syenite–granite intrusive stages, the chemical compositions of silicic magmas do not show significant difference (Fig. 7). Moreover, the order of emplacement for the AFS and PA granitoids remains the same.

The late Mesozoic PA plutonic and volcanic rocks, as represented by the gneissic granite from the Mangirtui pluton and the comendites from the Malo-Khamardaban volcanic structure (see Fig. 4), are chemically similar to their older equivalents. The compositions of the samples from the Mangirtui pluton fall within the field of earlier peralkaline granites (Figs. 5–8). The Early Cretaceous comendite has a spidergram similar to that of the peralkaline granite (Fig. 8B), but some distinctions with the older comendites can be observed. The Cretaceous Oshurkovo alkali-feldspar syenite is characterized by the

anomalously high contents of Ba (3000–7000 ppm) and Sr (2500–4500 ppm); as well as the enrichment in P<sub>2</sub>O<sub>5</sub> (0.12–0.23 wt.%). Such chemical characteristics are probably inherited from the nature of its parental magma (alkali monzonitic gabbro) and further enhanced by fractional crystallization (Litvinovsky et al., 2002b).

#### 4.2. Sm/Nd and Rb/Sr isotope data

The Sm/Nd and Rb/Sr isotope data are presented in Table 3 and are further illustrated in Fig. 9. It was noted recently (Jahn, 2004 and references therein) that PA and AFS granites of Central Asia commonly show highly fractionated REE patterns, sometimes with the lanthanide tetrad effect. This leads to enhanced Sm/Nd ratios and negative model ages (e.g., Jahn et al., 2001, 2004; Wu et al., 2002, 2004). Concerning the initial Sr isotope ratios, the uncertainty in *I*(Sr) calculation for individual samples increases with increasing <sup>87</sup>Rb/<sup>86</sup>Sr ratios. When <sup>87</sup>Rb/<sup>86</sup>Sr ratios are > 10, the induced errors in calculated *I*(Sr) become too large to yield significant *I*(Sr) values for petrogenetic interpretation (Wu et al., 2002; Jahn, 2004). In the following

Table 2 (continued)

Sample no.	727	728	A516a	KH14	866	870	3008	37-1	68-1	65-1	14	B611	A102	B590	A127	M77
Rock	PA syenite			PA syenite		AFS syenite		Monzodiorite	Monzonite	AFS syenite		PA granite			Comendite	
<i>Late Mesozoic stage</i>																
<i>Kharitonovo Complex</i>								<i>Oshurkovo pluton</i>				<i>Mangirtui pluton</i>				<i>Malo-Khamardaban</i>
SiO <sub>2</sub> (%)	66.56	64.94	66.1	63.3	66.06	62.42	71.15	44	53.00	62.0	66.24	71.2	73.8	71	72.3	73
TiO <sub>2</sub>	0.89	0.91	0.56	1.27	0.73	0.88	0.34	3.24	1.97	0.58	0.48	0.38	0.4	0.44	0.13	0.12
Al <sub>2</sub> O <sub>3</sub>	15.04	16.18	16.3	16.23	15.73	18.59	14.56	13.1	16.85	19.0	16.1	12.8	11.94	13.6	13.52	13.25
Fe <sub>2</sub> O <sub>3</sub>	2.07	2.01	0.2	2.61				5.98	3.01	1.88	1.69	1.34	1.95	2	1.44	1.71
FeO	1.41	1.1	2.88	1.68	4.29	2.93	2.64	4.21	4.45	1.32	1.29	1.81	1.55	0.97	1.25	1.18
MnO	0.17	0.14	0.1	0.15	0.1	0.12	0.08	0.09	0.09	0.02	0.03	0.17	0.2	0.17	0.15	0.14
MgO	0.62	0.75	0.36	0.72	0.44	0.77	0.14	7.1	3.38	0.50	0.63	0.22	0.24	0.2	0.09	0.12
CaO	0.59	0.56	0.14	1.43	0.45	1.21	0.3	12.2	5.55	0.44	0.62	0.56	0.48	0.26	0.43	1.12
Na <sub>2</sub> O	6.49	6.71	6.5	5.46	5.9	5.35	4.62	3.32	4.57	6.00	5.34	5.03	4.15	5.6	5.33	5.5
K <sub>2</sub> O	5.45	5.72	5.5	6.09	5.65	6.2	5.33	2.39	3.94	6.83	6.19	4.91	4.7	5.06	4.52	4
P <sub>2</sub> O <sub>5</sub>	0.1	0.11	0.09	0.28	0.06	0.19	0.06	2.79	1.41	0.13	0.23	0.04	0.03	0.04	0.03	0.08
LOI	0.46	0.28	1.02	1.08	0.3	0.56	1	1.26	1.39	0.81	1.34	1.1	0.35	0.9	0.58	0.36
Total	99.85	99.41	99.75	100.3	99.71	99.22	100.22	99.68	99.61	99.51	100.18	99.56	99.79	100.24	99.77	100.58
<i>Trace elements (in ppm)</i>																
Rb	76	51	86	120	177		377	11	28	55	120	125	120	100	336	370
Sr	31	6	54	65	10		36	5100	5200	3100	2444	19	26	65	34.2	21
Ba	225	27	250	540	65		120	3200	4900	3900	3081	41	70	240	59.4	430
Nb	26	16	27	25	18.3		46	5	130	1.00	17	11	14	28	107.4	120
Ta	1.77	0.72			0.98		1.34		8			0.46			6.3	3.77
Th	11	2.19		19						1					36.24	22
U		0.83		4											8.31	5.49
Zr	990	290	890	520	228		503	130		370	290	590	750	1020	468	470
Hf	17.6	5.7								6.8		12.0			17.9	11.8
Y	61	31	38	50	37		56	24	13	4	9	28	20	63	25.1	33
Ga	31	30			27		29					26			33	29
La	53	43		96	48	30	62	85	62	47		56			49	71
Ce	119	91		210	101	55	132	240	150	93		120			86	157
Pr	14.1	12.8										13.9			8.8	19.1
Nd	56	53		90	49	23	50	160	92	39		51			24	68
Sm	10.9	9.6		15	8.4	6.8	8.3	21	12	4.2		8.8			3.8	12.4
Eu	1.98	1.56		3.5	1.3	2.1	0.51	6	3.9	2.2		0.73			0.3	0.73
Gd	10.1	8.2			7.4	8.1	5.2					8.1			3.7	10.4
Tb	1.8	1.2		2.2				1.5	0.74	0.23		1.18			0.57	1.73
Dy	10.7	6.4			5.0	6.6	3.6					6.9			3.4	10.1
Ho	2.28	1.26										1.23			0.72	2.01
Er	6.5	3.48										3.74			2.24	5.65
Tm	1.02	0.49			0.33	0.57	0.28					0.59			0.37	0.81
Yb	6.64	3.17		4.9	2.11	3.2	1.62	0.72	0.39	0.28		3.7			2.64	5.09
Lu	1.01	0.49		0.73	0.3	0.5	0.23	0.05	0.05	0.03		0.65			0.39	0.72
Eu/Eu*	0.58	0.54		0.71	0.5		0.24	0.99	1.14	1.86		0.27			0.25	0.2
NK/A	1.10	1.06	1.02	0.96	1.01	0.83	0.92	0.61	0.90	0.91	0.96	1.06	1.00	1.08	1.01	1.01
A/CNK	0.88	0.91	0.97	0.96	0.97	1.12	1.07	0.68	1.00	1.08	1.00	0.91	0.97	0.91	0.96	0.92
A/NK	0.91	0.94	0.98	1.04	0.99	1.20	1.09	1.63	1.43	1.10	1.04	0.94	1.00	0.93	0.99	0.99

petrogenetic discussion, we will restrict our use of  $I(\text{Sr})$  values obtained only from low  $^{87}\text{Rb}/^{86}\text{Sr}$  samples, and, in some cases, from isochrons of plutons which yielded Rb/Sr ages comparable with the U–Pb zircon ages (Table 1).

As a whole, the granitoids and mafic plutonic rocks equally show a similar variation in  $\varepsilon\text{Nd}(T)$  value from stage 1 to stage 3. Negative  $\varepsilon\text{Nd}(T)$  values from  $-1$  to  $-5$  are characteristic of the Early Permian mafic and felsic rocks (Fig. 9A and C). The Early Mesozoic rocks (Stage 2) have higher  $\varepsilon\text{Nd}(T)$  values, from  $-1.5$  to  $+4$ , with dominantly positive values. Negative  $\varepsilon\text{Nd}(T)$  values were observed only in the oldest rocks from this stage (e.g. the Kharitonovo complex). The late Mesozoic rocks (Stage 3), like the Early Permian granitoids (Stage 1), have negative  $\varepsilon\text{Nd}(T)$  values of  $-2$  to  $-3.5$ .

Nd model ages ( $T_{\text{DM}}$ ) were calculated with a two-stage model for felsic rocks (Keto and Jacobsen, 1987; DePaolo et al., 1991) and a single-stage model for mafic rocks. The data in Table 3 show the variation of model ages roughly mirroring that of the  $\varepsilon\text{Nd}(T)$  values for different stages: 1000–1400 Ma for stage 1; 700–1100 Ma for stage 2, and 900–1200 Ma for stage 3.

There is little difference in  $\varepsilon\text{Nd}(T)$  and  $T_{\text{DM}}$  between the felsic and mafic rocks, between the PA and AFS granitoids, as well as between the syenite and granite formed in the same stage (Fig. 9A and B). Note that the similar  $\varepsilon\text{Nd}(T)$  values are characteristic of the different lithological associations of mafic and felsic rocks (Table 3): volcanic trachybasalt and comendite (the Tsagan–Khurtei volcanic suite; Early Mesozoic stage); peralkaline syenite and cross-cutting trachyandesite dykes (the Bryansky Complex; Early Permian stage); and K-rich gabbro and syenite (the Ust–Khilok pluton; Early Permian).

The  $I(\text{Sr})$  values in felsic and basic rocks from 5 plutons overlap significantly (Table 3). Though the  $I(\text{Sr})$  values calculated for individual granitoid samples show a fairly wide range, data obtained from the Rb/Sr isochrons for a number of plutons (Bryansky, Khorinsk, Kharitonovo in Table 1) proved to be rather similar, varying from 0.7053 to 0.7064. The values are close to those of mafic rocks (Table 3) and almost completely overlap with the range given for Late Paleozoic and Mesozoic basalts from the bimodal volcanic suites of Transbaikalia, 0.7043–0.7061 (Yarmolyuk et al., 1998, 2001, 2002).

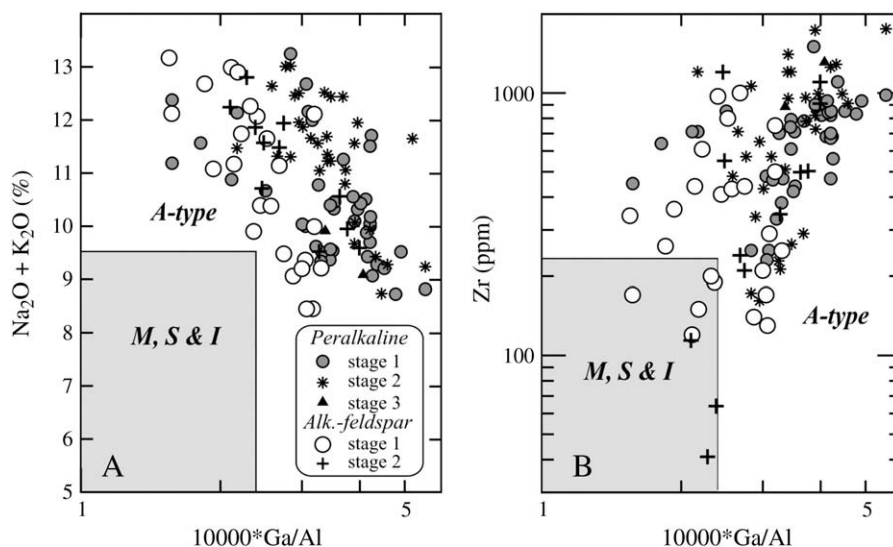


**Fig. 5.** Geochemical plots of the Early Permian (Stage 1) and Late Triassic (Stage 2) syenite–granite suites and peralkaline granite from the Mangirtui pluton (Late Jurassic, stage 3): A and B,  $10000 \text{ Ga/Al}$  vs  $(\text{Na}_2\text{O} + \text{K}_2\text{O})$  and  $10000 \text{ Ga/Al}$  vs Zr plots of Whalen et al. (1987); Abbreviations: M, S & I represent mantle, S-type and I-type granites, respectively.

#### 4.3. Results of melt inclusion study

Melt inclusions trapped by growing magmatic minerals can provide considerable information on the composition, temperature and volatile content of magmas (Roedder, 1979; Reyf, 1997; Thomas and Klemm, 1997; Webster and Rebert, 2001). We performed a melt inclusion study for the PA syenite, granite and comendite of the Bryansky Complex (ca. 280 Ma; Litvinovsky et al., 2002a) and for the comendite, trachyte, trachybasalt from the Tsagan–Khurtei volcanic suite (ca. 210 Ma). Most of the inclusion-bearing phenocrysts are quartz. However, in the porphyritic nordmarkite from a contact chilled zone, melt inclusions in clinopyroxene were studied, whereas in basic rocks, melt inclusions in olivine and clinopyroxene phenocrysts were analyzed.

The results are presented in Table 4. The data indicate that the temperature of nordmarkite magma ( $930 \text{ }^\circ\text{C}$ ) at the depth of the Bryansky Complex emplacement is significantly higher than that of PA granite magma ( $760\text{--}790 \text{ }^\circ\text{C}$ ). Unusually high homogenization temperatures ( $T_{\text{hom}}$ ), up to  $1100 \text{ }^\circ\text{C}$ , are also found for comendites of the Early Permian and Late Mesozoic eruption stages, whereas a broad range of  $T_{\text{hom}}$  ( $750\text{--}1100 \text{ }^\circ\text{C}$ ) was measured for quartz phenocrysts. The  $T_{\text{hom}}$  in three comendite samples (B440, B444, B456) seems to show an inverse correlation with the  $\text{H}_2\text{O}$  content (Table 4). The  $\text{H}_2\text{O}$  content increases from 0.4 to 2.85 wt.%, whereas the  $T_{\text{hom}}$  decreases from  $1100 \text{ }^\circ\text{C}$  to  $750\text{--}780 \text{ }^\circ\text{C}$ . Regarding the halogens, all peralkaline silicic magmas contain enhanced Cl concentrations (0.2–0.3 wt.%), but show uneven distribution of F, from  $<0.3 \text{ wt.}\%$  (below the limit of detection) to  $\sim 1.6 \text{ wt.}\%$ . High F concentration is observed for PA granite with low  $T_{\text{hom}}$  and for comendite with moderate  $T_{\text{hom}}$  (sample A447-5).

## 5. Discussion

#### 5.1. Tectonic setting and emplacement periods of the granitoids

The fact that the three stages of PA and AFS granitoid magmatism occurred within the Mongolian–Transbaikalian Belt during a period of 120 My is rather unusual. In other belts shown in Fig. 1 only one or two stages are recognized. Also uncommon is the emplacement of similar magmatic sequences separated by a time interval of  $\sim 50 \text{ Ma}$ , in the Early Permian and Late Triassic. To account for these facts, we discuss below the main late Paleozoic magmatic and tectonic events in the eastern half of the CAOB, with special reference to the MTB and adjacent terranes.

By the end of the Carboniferous, the CAOB was a vast accreted continental margin of the “Siberian continent” (= Siberian craton + accreted CAOB; Mossakovsky et al., 1994; Kovalenko et al., 2004; Buslov et al., 2004; Windley et al., 2007). The continental margin formed in two stages, the Early Paleozoic (“Caledonian”) and the Late Paleozoic (“Hercynian”), as a result of northward subduction of the oceanic lithosphere (Kovalenko et al., 2004; Windley et al., 2007). The Solonker suture of Inner Mongolia represents the southern termination of the CAOB (Fig. 1; Sengör et al., 1993; Xiao et al., 2003, 2004). In the Late Carboniferous and Early Permian an oceanic basin (Paleo-Asian ocean) still existed to the south of the active continental margin (present day coordinates). In the northeastern part of the CAOB the Mongol–Okhotian oceanic basin extended from the northeastern Mongolia to the Okhotian Sea (Fig. 1).

The generation of the PA and AFS granitoids is closely linked with the continental rifting of the CAOB. The Late Paleozoic–Early Mesozoic “Central Asia Rift System”, a term proposed by Kovalenko et al. (2004), stretches over 5000 km from southeastern Kazakhstan to the Russian Far East, and the granite belts mark the sites of the large rifts (Fig. 1).

Figs. 1 and 2 show that three stages of highly alkaline granitoid emplacement can be recognized in the central and eastern parts of the CAOB: Late Paleozoic ( $\sim 320\text{--}260 \text{ Ma}$ ), Early Mesozoic ( $230\text{--}190 \text{ Ma}$ )

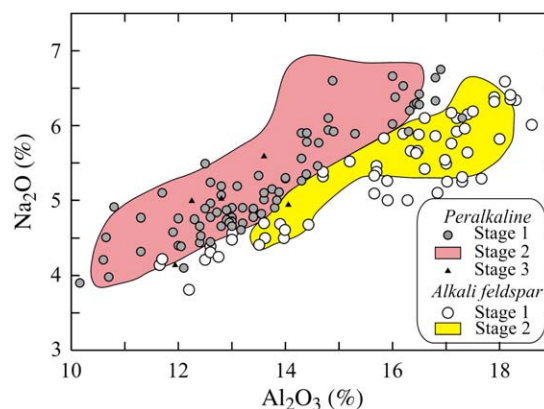


**Fig. 6.**  $\text{Al}_2\text{O}_3$  vs  $\text{Na}_2\text{O}$  plot showing that the chemical compositions of the same rock types from different stages overlap almost completely. Peralkaline granite of the Mangirtui pluton (stage 3, Late Jurassic) also falls in the peralkaline granite field.

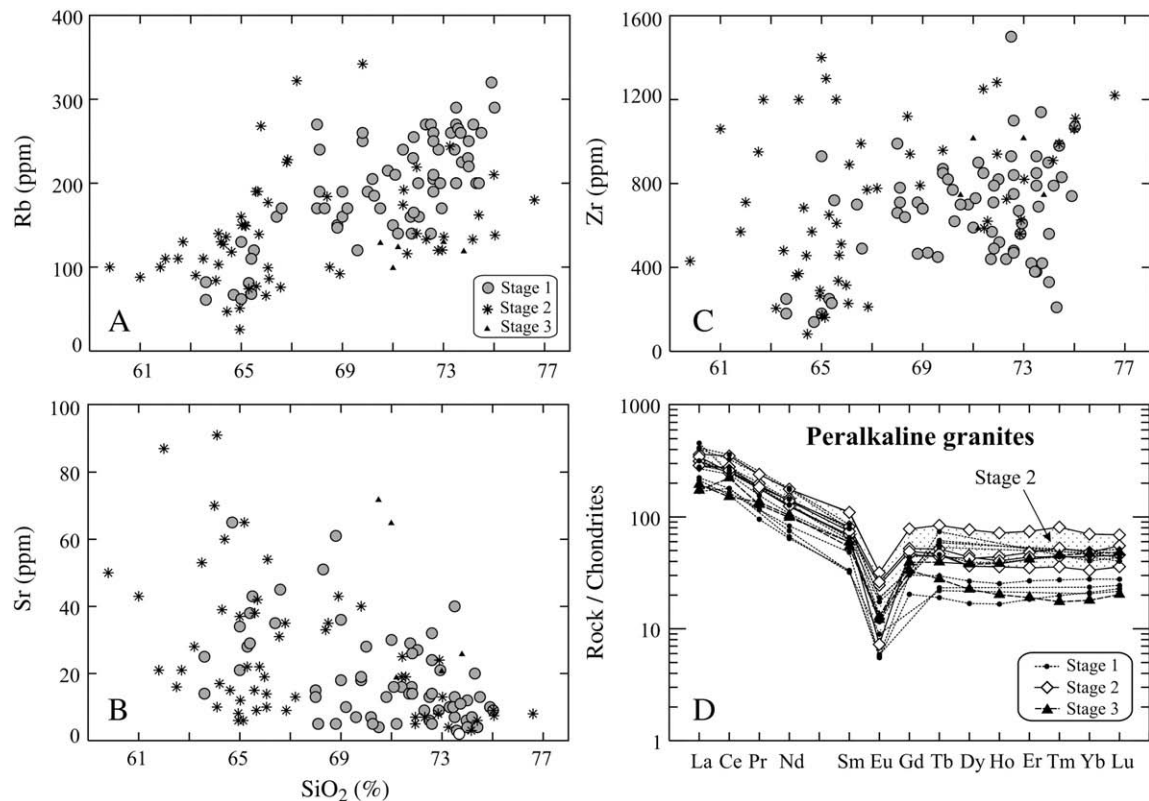


**Fig. 7.** A to C,  $\text{SiO}_2$  vs Rb, Sr, Zr plots for peralkaline syenite and granite of Early Permian (stage 1) and Late Triassic (stage 2) and for granite from the Mangirtui pluton (Late Jurassic, stage 3). D, REE patterns for Early Permian (Stage 1) and Late Triassic (Stage 2) peralkaline granites and for Late Jurassic (Stage 3) peralkaline granite (the Mangirtui pluton).

and Late Jurassic to Early Cretaceous (160–120 Ma). These stages are essentially similar to that recognized in the MTB alone, though the intervals of magmatic activity are slightly longer. Note that in the western part of the CAOB (central and eastern Kazakhstan) PA and AFS granitoids are also abundant and they have been studied in some detail (Leontyev et al., 1981; Yermolov et al., 1988; Heinhorst et al., 2000), but reliable isotopic age data are very scarce. Based on the field relations, the available paleontological data and K–Ar dates, two stages of magmatism, Early Permian and Permian–Triassic, have been recognized in the region (Leontyev et al., 1981).

#### 5.1.1. The Late Paleozoic magmatism (Stage 1)

The emplacement of Late Paleozoic highly alkaline granitoids and bimodal volcanic rocks began at 314–318 Ma. So far, these rocks are known only in two places in the Noyon and Tost Ranges of southern Mongolia (Table 5; belt 8 in Fig. 1). Most Late Paleozoic PA and AFS granites and syenites in eastern CAOB were emplaced during the period of 300–280 Ma (Figs. 1 and 2; Tables 1 and 5). In the Great Xing'an Mountains and Gobi–Tien Shan belts almost all dated plutons are late Carboniferous to Early Permian, from 295 to 270 Ma (Fig. 1). To the north of the Gobi–Tien Shan belt, in central Mongolia and eastern Junggar (Fig. 1, belts 5, 6 and 7), PA granite plutons of 295–275 Ma are also present (Table 5; Fig. 1). Further to the north in the MTB (Fig. 1, belt 1) the two largest igneous complexes, Bryansky (Fig. 3) and Khorinsk (Fig. 2), formed between 285 and 270 Ma (Fig. 2; Table 1). Thus, the Late Carboniferous–Early Permian stage of highly alkaline granitoid magmatism was manifested simultaneously in all granite belts of the CAOB. However, the tectonic setting during the granite emplacement was not the same in all belts.

The Mongolian–Transbaikalian belt formed within a continental plate more than 1000 km to the north from the border of the Paleo-Asian ocean, but only few hundred kilometers from the Mongol–Okhotian oceanic basin. The period of massive granitoid emplacement started with several pulses of high-K calc-alkaline granite and quartz monzonite

making up one of the largest granitoid complexes in the CAOB, the Angara–Vitim batholith (150,000 km<sup>2</sup> in area), during 330 Ma to 285 Ma. This stage was followed (with partial overlap in time) by voluminous intrusion of two-feldspar monzogranite, syenogranite and quartz syenite during 305–285 Ma (Litvinovsky et al., 1999; Tsygankov et al., 2007). Finally, the emplacement of Early Permian PA and AFS granitoids completed the 60 My-long period of post-collisional magmatic activity in Transbaikalia (Yarmolyuk et al., 2005; Tsygankov et al., 2007 and references therein).

The Gobi–Altai belt (Fig. 1, belt No. 5) was formed in within-plate setting during the Permian (275–260 Ma; possibly to 250 Ma). The tectonic setting of the Great Xing'an granite belt (Fig. 1, belt No. 2) is debatable. According to Wu et al. (2002 and references therein), the emplacement of highly alkaline granites followed the collision of the Siberian Plate and the Xing'an Block. On the other hand, the tectonic reconstructions by Khanchuk and Mikhailov (1989), Zonenshine and Kuzmin (1993), and Parfenov et al. (2003) showed that in the Permian the Xing'an Block was part of the Burean massif located far to the south, on the opposite side of the Mongol–Okhotian ocean. If this is the case, we may suggest that the Early Permian peralkaline granite belts were produced and evolved simultaneously on the both sides of the paleo-ocean.

#### 5.1.2. The Early Mesozoic magmatism (Stage 2)

The Early Mesozoic highly alkaline granitoids are also abundant throughout the CAOB. Reliable age data, ranging from 230 to 190 Ma, have been obtained for some terranes in Transbaikalia, eastern Mongolia and northeastern China (Tables 1 and 5; Figs. 1 and 2).

The central and northeastern parts of the MTB are considered by Yarmolyuk et al. (2002) as a northern portion of the Early Mesozoic Mongol–Transbaikalian igneous province (Fig. 1). The core of the province is occupied by the Khentei–Daurian batholith, which is made up mostly of high-K calc-alkaline granite, whereas the border zones are rifts that controlled the location of PA and AFS granitoids. The calc-alkaline and alkaline granites were emplaced during the same time

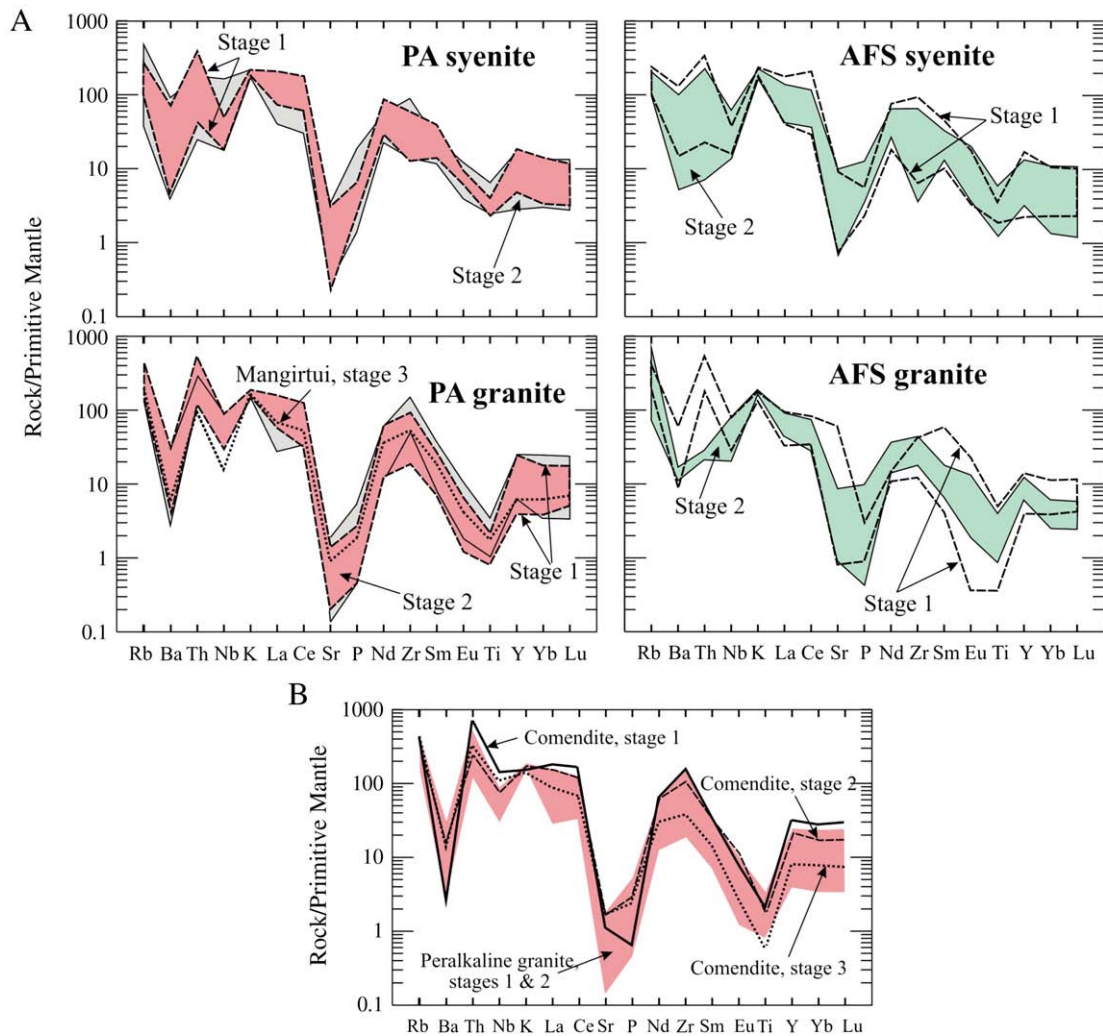


**Fig. 8.** Primitive-mantle-normalized spidergrams for the plutonic and volcanic felsic rocks. A, Early Permian (stage 1, open field) and Late Triassic (stage 2, gray and dotted fields) PA and AFS syenites and granites. For clarity, only the maximum and minimum abundances are shown for each rock type (Tables 2 and S1–S4, Supplementary data). These plots demonstrate a great similarity of the same rock types of different ages. B, comendites of the three stages and the compositional field of peralkaline granites (gray field). Normalizing values are from Sun and McDonough (1989).

span of 227–207 Ma. Consequently, the Late Triassic AFS and PA granitoids of the MTB were actually part of the large igneous province as defined by Yarmolyuk et al. (2002).

The emplacement of the PA and AFS granites in the Zhangguangcai belt (NE China) occurred in a within-plate setting, soon after the collision of the Songliao–Jiamusi block with the North China craton during the Jurassic (Wu et al., 2002, 2007b).

### 5.1.3. The Late Mesozoic magmatism (Stage 3)

Extensive within-plate igneous activity was manifested in several provinces of the CAOB during 170–120 Ma (Yarmolyuk et al., 1998; Kovalenko et al., 2004). Peralkaline and alkali feldspar granites were emplaced in central CAOB (western Transbaikalia, southern Hangei and eastern Mongolia) as well as in NE China (Jahn et al., 2001; Wu et al., 2002, 2003a,b, 2004; see Fig. 4, Inset). The volcanic domains overlap significantly with the Late Paleozoic and Early Mesozoic granite belts described above. Together they form the “Central East Asia intraplate province”. This province is characterized by the occurrence of trachybasalt, trachyandesite, phonolite, trachyte, and subordinate trachyrhyolite and ongonite. These rocks are mainly confined to large tectonic depressions (Fig. 4). Along with Jurassic and Cretaceous depressions, a number of metamorphic core complexes also evolved within the Central East Asia intraplate province (Windley et al., 2007; Donskaya et al., 2008). A number of small Late Jurassic

(~150 Ma) peralkaline granite plutons were spaced with the metamorphic core complexes. The next stage of peralkaline silicic magmatism occurred in the Early Cretaceous (120–130 Ma), which was represented in Transbaikalia by a small amount of comendite and pantellerite (Fig. 4). In NE China, four Early Cretaceous PA and AFS granite plutons have been found (Fig. 1; Table 5). These granites are related to rifting that followed the subduction of the Paleo-Pacific Plate in Cretaceous (Wu et al., 2002, 2005).

## 5.2. Mantle-derived component in the PA and AFS granitoids of the MTB

### 5.2.1. Isotopic arguments

A-type granitoids are known to have multiple origins, but in many cases, mantle-derived material, rather than the continental crust material, seems to have played the dominant role in their petrogenesis (e.g. Wickham et al., 1995; Liégeois et al., 1998; Wu et al., 2002; Bonin, 2004, 2007; Jahn, 2004). In the present study, the granitoids from stages 1 and 3 have slightly negative  $\epsilon_{\text{Nd}}(T)$  values,  $-1$  to  $-5$  and  $-2$  to  $-3.5$ , respectively, whereas slightly positive values ( $-1$  to  $+4$ ; with the great majority from  $0$  to  $+4$ ) prevail in stage 2 rocks (Fig. 9). Note that the coeval, mantle-derived gabbros and basalts from the bimodal volcanic suites associated with the highly alkaline granitoids also show similar negative  $\epsilon_{\text{Nd}}(T)$  values, from  $-0.5$  to  $-4.5$ , and similar model ages (Fig. 9; Table 3). In fact, Yarmolyuk

**Table 3**  
Sr–Nd isotope data of Late Paleozoic and Mesozoic PA and AFS granitoids and related volcanic rocks from the Mongolian–Transbaikalian Belt.

Sample no.	Rock	Locality (pluton name)	Age (Ma)	Rb	Sr	<sup>87</sup> Rb/ <sup>86</sup> Sr	<sup>87</sup> Sr/ <sup>86</sup> Sr	2 σ <sub>m</sub>	( <sup>87</sup> Sr/ <sup>86</sup> Sr) <sub>T</sub>	Sm	Nd	<sup>147</sup> Sm/ <sup>144</sup> Nd	<sup>143</sup> Nd/ <sup>144</sup> Nd	2 σ <sub>μ</sub>	εN (0)	f (Sm/ Nd)	εN (T)	T <sub>DM</sub> <sup>-1</sup> (Ma)	T <sub>DM</sub> <sup>-2</sup> (Ma)
<i>Early Permian stage</i>																			
B 626	AFS syenite	Bryansk	280	105	55.8	5.48	0.726765	7	0.70494	16.37	97.70	0.1013	0.512293	4	−6.7	−0.49	−3.3	1161	1349
B 626-1	AFS syenite	Bryansk	280	112	58.0	5.62	0.727423	8	0.70502	9.61	62.43	0.0931	0.512301	5	−6.6	−0.53	−2.9	1072	1325
B425	AFS granite	Bryansk	280	187	47.0	11.6	0.749261	7	0.70323	2.09	14.73	0.0858	0.512320	4	−6.2	−0.56	−2.2	989	1284
B627	PA syenite	Bryansk	280	142	45.5	9.03	0.739562	8	0.70359	18.74	113.46	0.0999	0.512317	4	−6.3	−0.49	−2.8	1115	1308
B388	PA granite	Bryansk	280	204	7.1	86.0	1.037942	10	0.69543	10.92	56.44	0.1170	0.512364	4	−5.3	−0.41	−2.5	1237	1256
A447-4	comendite	Bryansk	285	265	39.0	19.8	0.785460	8	0.70517	21.81	116.14	0.1135	0.512356	4	−5.5	−0.42	−2.5	1207	1265
B382-2	comendite	Bryansk	285	275	14.1	57.8	0.938820	10	0.70443	15.35	76.07	0.1220	0.512342	4	−5.8	−0.38	−3.1	1341	1299
B167-3	trachybasalt	Bryansk	285	53.6	1241	0.125	0.705945	8	0.70544	7.60	39.12	0.1174	0.512436	4	−3.9	−0.40	−1.1	1130	1142
B385	trachyandesite	Bryansk	285	112	620	0.524	0.708063	7	0.70594	5.93	34.36	0.1043	0.512295	5	−6.7	−0.47	−3.3	1191	1350
B386	trachyandesite	Bryansk	285	125	639	0.565	0.707993	6	0.70570	5.77	33.04	0.1056	0.512290	5	−6.8	−0.46	−3.5	1211	1359
M-347	AFS syenite	Khorinsk	280	130	30.7	12.3	0.751267	10	0.70226	10.18	62.51	0.0985	0.512295	4	−6.7	−0.50	−3.2	1130	1342
3070	AFS granite	Khorinsk	280	215	37.0	16.9	0.768745	7	0.70152	7.98	44.69	0.1080	0.512311	5	−6.4	−0.45	−3.2	1209	1329
M-340	PA granite	Khorinsk	280	233	5.4	130.9	1.175625	19	0.65401	5.06	30.63	0.1000	0.512352	5	−5.6	−0.49	−2.1	1069	1253
479	PA granite	Khorinsk	280	219	7.5	87.1	1.018060	8	0.67089	6.07	35.98	0.1020	0.512253	4	−7.5	−0.48	−4.1	1223	1414
M-350	PA granite	Khorinsk	280	147	7.0	62.6	0.943791	12	0.69441	7.20	38.91	0.1119	0.512379	4	−5.1	−0.43	−2.0	1154	1226
M-487	trachybasalt	Khorinsk	285	96.8	630	0.444	0.706933	7	0.70513	6.14	31.02	0.1197	0.512480	6	−3.1	−0.39	−0.3	1086	1075
M-342	trachyandesite	Khorinsk	285	43.0	641	0.194	0.705841	7	0.70505	5.78	29.22	0.1196	0.512488	7	−2.9	−0.39	−0.1	1072	1062
M-492	AFS rhyolite	Khorinsk	285	260	10.3	74.9	0.978381	15	0.67465	6.74	31.91	0.1276	0.512327	6	−6.1	−0.35	−3.6	1455	1330
M-511	AFS rhyolite	Khorinsk	285	208	20.4	29.8	0.831608	12	0.71057	8.95	45.96	0.1177	0.512357	4	−5.5	−0.40	−2.6	1257	1269
M-501	syenite, country rock	Khorinsk	280	50.2	393	0.370	0.706927	6	0.70545	5.43	34.99	0.0938	0.512311	6	−6.4	−0.52	−2.7	1066	1310
530	AFS syenite	Ubur-Tashir*	280	82	618	0.384	0.708926	11	0.70740	4.00	21.00	0.1152	0.512415	6	−4.4	−0.41	−1.4	1136	1172
536	AFS granite	Ubur-Tashir*	280	425	12	108.3	1.285644	43	0.85434	12.00	59.00	0.1230	0.512279	5	−7.0	−0.37	−4.4	1461	1401
B341	syenite	Ust'-Khilok	280	122	400	0.883	0.709423	13	0.70591	11.00	68.00	0.0978	0.512246	7	−7.6	−0.50	−4.1	1188	1419
B361-20	syenite	Ust'-Khilok	280	52.9	148	1.03	0.711615	9	0.70749	3.30	17.49	0.1141	0.512238	6	−7.8	−0.42	−4.9	1393	1454
B111	monzonite	Ust'-Khilok	280	48.9	1095	0.129	0.706773	10	0.70626	6.50	36.31	0.1082	0.512263	7	−7.3	−0.45	−4.2	1280	1406
B342	alk. gabbro	Ust'-Khilok	280	76	1500	0.147	0.706967	12	0.70638	11.00	57.00	0.1167	0.512263	5	−7.3	−0.41	−4.5	1391	1418
B517-3	alk. gabbro	Ust'-Khilok	280	34.2	1489	0.066	0.706025	10	0.70576	7.19	38.33	0.1134	0.512275	6	−7.1	−0.42	−4.1	1328	1394
B144	syenite	Nadeino	270	51.3	221	0.672	0.709797	10	0.70722	6.62	35.95	0.1113	0.512297	7	−6.7	−0.43	−3.7	1269	1356
<i>Early Mesozoic stage</i>																			
B440	comendite	Tsagan-Khurtei	210	217	19.4	32.6	0.789440	8	0.69204	11.43	61.28	0.1128	0.512670	4	0.6	−0.43	2.9	725	761
B444	comendite	Tsagan-Khurtei	210	135	18.2	21.6	0.763315	8	0.69879	18.74	100.50	0.1127	0.512676	4	0.7	−0.43	3.0	716	752
1/8a	comendite	Tsagan-Khurtei	210	162	12.2	38.8	0.820440	23	0.70444	12.10	66.70	0.1097	0.512625	7	−0.3	−0.44	2.1	770	829
1/6a	trachybasalt	Tsagan-Khurtei	210	12.7	988	0.037	0.704550	15	0.70444	6.09	30.09	0.1224	0.512632	7	−0.1	−0.38	1.9	865	835

1/7a	trachybasalt	Tsagan-Khurtei	210	10	1188	0.024	0.705060	12	0.70499	7.22	37.40	0.1167	0.512646	7	0.2	-0.41	2.3	792	805
B446-1	trachybasalt	Tsagan-Khurtei	210	16.9	1136	0.043	0.704340	8	0.70421	8.08	41.09	0.1189	0.512694	4	1.1	-0.40	3.2	734	731
A13	PA granite	Atha	210	174	7	73.8	0.972651	24	0.75231	3.80	17.00	0.1351	0.512657	6	0.4	-0.31	2.0	957	813
A13-1	PA granite	Atha	210	174	19	26.7	0.795791	10	0.71598	17.00	82.00	0.1253	0.512664	7	0.5	-0.36	2.4	839	788
L716	PA granite	Atha	210	160	6	78.6	0.901733	33	0.66695	11.00	65.00	0.1023	0.512622	7	-0.3	-0.48	2.2	723	824
L722	PA granite	Atha	210	150	17	25.7	0.780302	13	0.70352	12.00	70.00	0.1036	0.512619	5	-0.4	-0.47	2.1	736	831
L725	PA granite	Atha	210	150	9	48.9	0.841547	26	0.69565	11.00	64.00	0.1039	0.512616	6	-0.4	-0.47	2.1	742	836
L726	PA syenite	Atha	210	70	24	8.46	0.729413	14	0.70416	10.00	58.00	0.1042	0.512620	7	-0.4	-0.47	2.1	739	830
L727	PA syenite	Atha	210	83	30	8.02	0.729600	13	0.70564	12.00	65.00	0.1116	0.512652	5	0.3	-0.43	2.6	744	789
L728	PA syenite	Atha	210	60	8	21.8	0.759577	18	0.69444	11.00	65.00	0.1023	0.512634	4	-0.1	-0.48	2.5	707	805
A65	PA granite	Kuka*	210	110	14	22.9	0.785788	13	0.71738	6.00	30.00	0.1209	0.512556	10	-1.6	-0.39	0.4	976	955
A66	PA granite	Kuka*	210	148	14	30.9	0.803614	12	0.71141	6.00	32.00	0.1134	0.512585	6	-1.0	-0.42	1.2	859	898
ERM-400	PA granite	Yermakovka	226									0.1450	0.512506	6	-2.6	-0.26	-1.0	1427	1110
ERM-411	PA granite	Yermakovka	226									0.0616	0.512381	6	-5.0	-0.69	-1.1	771	1112
B69-1	Afs syenite	Ara-Bilutay*	230	186	225	2.39	0.710171	15	0.70234	10.00	67.00	0.0902	0.512515	5	-2.4	-0.54	0.7	784	979
B69-2	Afs syenite	Ara-Bilutay*	230	153	237	1.87	0.709431	15	0.70332	5.00	33.00	0.0916	0.512514	6	-2.4	-0.53	0.7	794	982
A519	PA syenite	Malo-Kunaley	220	43.3	22.1	5.66	0.724745	10	0.70703	5.33	28.23	0.1141	0.512689	7	1.0	-0.42	3.3	706	733
A516a	PA syenite	Malo-Kunaley	220	86	54	4.61	0.718594	11	0.70416	7.00	42.00	0.1008	0.512718	6	1.6	-0.49	4.3	584	668
KH14	Afs syenite	Kharitonovo	230	130	85	4.43	0.719194	10	0.70470	12.00	67.00	0.1083	0.512468	6	-3.3	-0.45	-0.7	986	1078
870	AFS syenite	Kharitonovo	230	65	89	2.11	0.714243	17	0.70733	14.00	77.00	0.1099	0.512513	5	-2.4	-0.44	0.1	936	1009
3008	AFS granite	Kharitonovo	230	272	30	26.5	0.795004	10	0.70846	4.80	31.00	0.0936	0.512336	8	-5.9	-0.52	-2.9	1033	1270
866	PA syenite	Kharitonovo	230	175	14	36.6	0.831658	12	0.71191	29.00	155.00	0.1131	0.512496	5	-2.8	-0.42	-0.3	991	1040
<i>Late Mesozoic stage</i>																			
34-1	monzonite	Oshurkovo	130	9.6	6310	0.0044	0.705120	6	0.70511	14.46	93.20	0.0938	0.512451	5	-3.6	-0.52	-2.0	889	1087
37-1	monzodiorite	Oshurkovo	130	13.3	4741	0.0081	0.705135	6	0.70512	25.11	153.10	0.0992	0.512437	5	-3.9	-0.50	-2.3	949	1114
65-1	AFS syenite	Oshurkovo	130	52.4	3065	0.0495	0.705470	6	0.70538	6.12	48.10	0.0769	0.512387	5	-4.9	-0.61	-2.9	851	1165
14	AFS syenite	Oshurkovo	130	119	2539	0.135	0.705667	8	0.70542	7.14	55.90	0.0772	0.512358	4	-5.5	-0.61	-3.5	885	1211
A102	PA granite	Mangirtui	150	76.2	9.4	23.5	0.762697	15	0.71250	5.45	33.40	0.0986	0.512427	7	-4.1	-0.50	-2.2	958	1131
B590	PA granite	Mangirtui	150	56.4	25.6	6.38	0.728695	13	0.71508	6.92	38.50	0.1087	0.512438	6	-3.9	-0.45	-2.2	1033	1127

Pluton names with star (\*) are given by assumed ages; Sample numbers with superscript "a", such as, 1/8a are after Yarmolyuk et al. (1999).

Model age calculation: (1)  $T_{DM-1}$  (one-stage Sm–Nd model age) is calculated assuming a linear Nd isotopic growth of the depleted mantle reservoir from  $\epsilon Nd(T) = 0$  at 4.56 Ga to +10 at the present time.

$T_{DM-1} = 1 / \lambda \ln \{ 1 + [ (^{143}Nd / ^{144}Nd)_s - 0.51315 ] / [ (^{147}Sm / ^{144}Nd)_s - 0.2137 ] \}$ , where  $s$  = sample,  $\lambda$  = decay constant of  $^{147}Sm$  ( $0.00654 \text{ Ga}^{-1}$ ).

(2)  $T_{DM-2}$  (two-stage model age) is obtained assuming that the protolith of the granitic magmas has a Sm/Nd ratio (or  $f_{sm}/Nd$  value) of the average continental crust (Keto and Jacobsen, 1987):  $T_{DM-2} = T_{DM1} - (T_{DM1} - t)(fcc - fs) / (fcc - f_{DM})$ , and  $f_{sm}/Nd = [ (^{147}Sm / ^{144}Nd)_s / (^{147}Sm / ^{144}Nd)_{CHUR} ] - 1$  where  $fcc$ ,  $fs$ , and  $f_{DM}$  are  $f_{sm}/Nd$  values of the average continental crust, the sample and the depleted mantle, respectively. In our calculation,  $fcc = -0.4$  and  $f_{DM} = 0.08592$  are used, and  $t$  = intrusive age of granite.

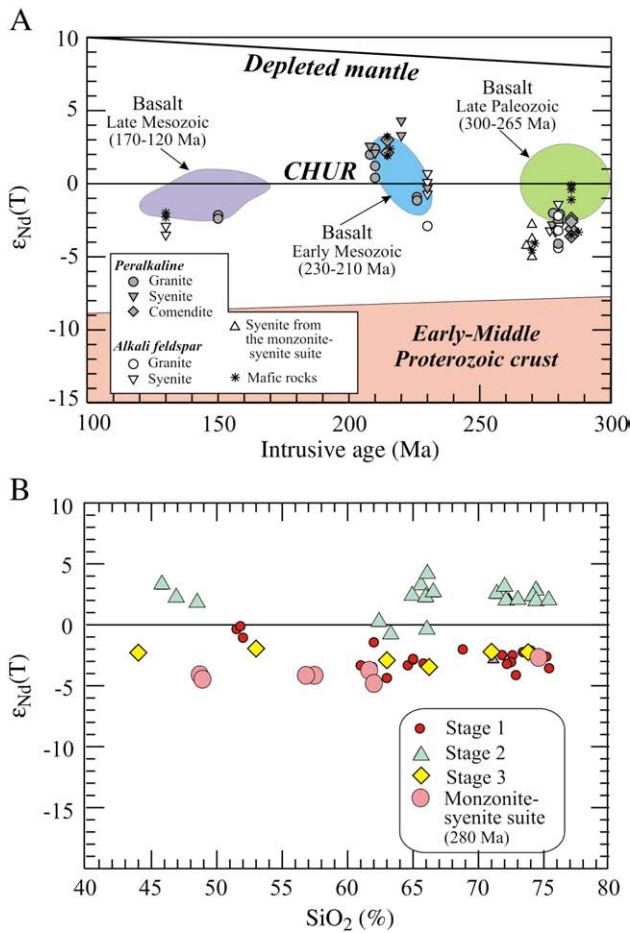


**Fig. 9.** A,  $\epsilon_{Nd}(T)$  vs intrusive age (Ma) diagram for the granitoids and mafic rocks from the MTB. Data for basalts are from Yarmolyuk et al. (1998; 2002). B,  $\epsilon_{Nd}(T)$  vs  $SiO_2$  plot for the same rocks as in A.

et al. (1998, 2002) have earlier reported that Late Paleozoic to Late Mesozoic K-rich basalts of the MTB are characterized by near-zero to slightly negative  $\epsilon_{Nd}(T)$  values (Fig. 9A). We interpret such an isotopic signature to be characteristic of the contemporaneous enriched mantle beneath the MTB.

As for the Sr isotopic compositions, a significant overlap in  $I(Sr)$  values is observed in granitoids, gabbros and basalts (Tables 1 and 3). Most samples, regardless of mafic or felsic compositions, have a limited  $I(Sr)$  range from 0.7053 to 0.7064. If only the data of rocks with  $^{87}Rb/^{86}Sr < 10$  are used, the range is also identical, from 0.7050 to 0.7060. The only possible exception is peralkaline gneissic granite from the Mangirtui pluton that was emplaced during formation of a metamorphic core complex in Late Jurassic. The calculated  $I(Sr)$  value for this rock type is 0.7151 (Table 3), which suggests involvement of a Precambrian crustal component.

Thus, radiogenic isotope data suggest that at each stage of magmatic activity highly alkaline silicic magmas were derived either from a mantle source or from mantle-derived mafic rocks in the lower crust. An enriched mantle source was likely responsible for the formation of the Early Permian and Late Mesozoic rocks, whereas a mildly depleted source was envisaged for the Early Mesozoic granitoids. The evidence of mantle-derived sources was corroborated by a study of oxygen isotopes in titanite and quartz from PA and AFS granitoids from Transbaikalia (Wickham et al., 1995; Litvinovsky et al., 1999). A detailed description of the analytical techniques is given in Wickham et al. (1996). These workers showed that  $\delta^{18}O$  values in Ttn, Qtz and WR samples from AFS quartz syenite and PA granite of the

Kharitonovo pluton (see Fig. 2) were mantle-like: 2.8–3.8‰ (Ttn), 7.6–8.1‰ (Qtz), and 6.2–7.6‰ (WR). At the same time, in granites making up the Late Carboniferous Angara–Vitim batholith the  $\delta^{18}O$  values are characterized by dominantly crustal source: 7.2–7.6‰ (Ttn), 11.1–13.4‰ (Qtz), and 10.7–12.2‰ (WR).

5.2.2. Geological evidence

In a recent review Bonin (2007) drew attention to important non-isotopic evidence for the mantle origin of A-type granites. In particular, he pointed out that large volumes of PA granite and syenite formed in regions with oceanic crust (i.e. Kerguelen Archipelago) and stressed that no peralkaline granite liquids had been produced experimentally from crustal materials, and no leucosomes of A-type composition had been detected in magmatic terranes. The data presented in this paper reinforce the non-isotopic arguments for the “mantle origin” of the AFS and PA granitoids of the MTB.

It is shown in Fig. 1 that the PA and AFS granitoids, along with the associated bimodal volcanic rocks, form a network of very large belts controlled by the Central–Asian Rift System. Although the belts are superimposed on different terranes or crustal blocks (e.g., Precambrian microcontinental blocks; the early Paleozoic “Caledonian” and the late Paleozoic “Hercynian” terranes), there is no correlation between the nature and age of the terrane and the composition of the granitoids. Moreover, the granitoids emplaced in the three stages (285–270 Ma, 230–210 Ma and 150–120 Ma) have broadly similar compositions (Figs. 5–8). This concerns not only the granites, which

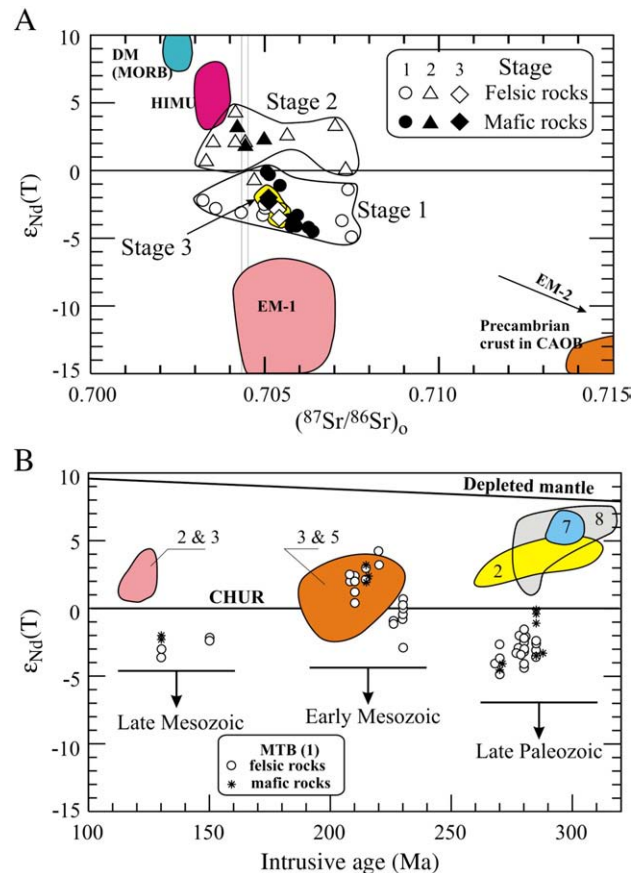


**Fig. 10.** A,  $\epsilon_{Nd}(T)$  vs  $(^{87}Sr/^{86}Sr)_0$  diagram for three stages of highly alkaline granitoid magmatism in the MTB. The principal mantle components of Zindler and Hart (1986) are shown for reference. The field of the Proterozoic crust in the CAOB is after Kovalenko et al. (2004). B,  $\epsilon_{Nd}(T)$  vs intrusive age (Ma) diagram for the three stages of Late Paleozoic to Late Mesozoic PA and AFS granitoids and related mafic rocks from the CAOB (based on the data from Tables 3 and 5). Numbers of the granite belts as in Fig. 1 and Table 5.

**Table 4**

Homogenization temperature ( $T_{\text{hom}}$ , °C) and fluid contents in melt inclusions in phenocrysts of quartz and mafic minerals from the plutonic and volcanic rocks.

Sample number	Rock	$T_{\text{hom}}$ , °C	Fluid component		
			F	Cl	H <sub>2</sub> O
<i>Bryansky Complex (280 Ma)</i>					
B527-6	Nordmarkite (Cpx)	930–940	–	2.2	n.d.
B389	Peralkaline granite	760–790	1.6	2.6	n.d.
B388	Peralkaline granite	700–720	1.4	2.5	n.d.
M250-7	Comendite	1100	–	0.14	n.d.
B603-4	Comendite	1090	–	0.65	n.d.
B600-1	Comendite	1090	0.66	0.19	n.d.
A447-7	Comendite	980–1020	–	0.26	n.d.
A447-5	Comendite	920–930	n.d.	n.d.	n.d.
B382-2	Comendite	850–880	n.d.	n.d.	n.d.
A452-1	Comendite	860–880	n.d.	n.d.	n.d.
<i>Tsagan-Khurtei volcanic field (212 Ma)</i>					
440 <sup>a</sup>	Comendite	1030–1100	0.85	0.29	0.4
450	Comendite	1050–1100	n.d.	n.d.	n.d.
444 <sup>a</sup>	Comendite	885–920	0.6	0.25	2.35
443	Comendite	870	n.d.	n.d.	n.d.
456 <sup>a</sup>	Granite porph	750–780	–	0.12	2.85
448	Essexite (Cpx)	1130–1160	n.d.	n.d.	n.d.
446-1	Trachybasalt (Ol)	1280–1320	n.d.	n.d.	n.d.

Cpx, clinopyroxene; Ol, olivine; the rest are quartz crystals.

–, below the detection limit; the detection limit for F < 0.3 wt.%, for Cl = 0.05–0.07 wt.%, for H<sub>2</sub>O < 0.02 wt.%.

n.d., not determined.

Major and selected trace element compositions of the studied melt inclusions are in Litvinovsky et al. (2002a) and Kuzmin et al. (1999).

<sup>a</sup> Samples in which fluids were determined in the unheated melt inclusions.

can be regarded as highly evolved products, but also Qtz-bearing syenites which have compositions far away from the granite eutectics. Such particular chemical characteristics of the granitoids and the control of their distribution by large continental rift zones suggest the dominant role of the “mantle component” in the generation of these silicic magmas.

It was shown that quartz-bearing to quartz syenites are abundant both in the PA and AFS granitoid suites of the MTB (Fig. 3; Litvinovsky et al., 1999, 2002a). The common presence of syenites is noted in highly alkaline granitoid suites throughout the CAOB (Leontyev et al., 1981; Yarmolyuk et al., 2002, 2005) and in many A-type granite localities of the world (e.g. Whalen et al., 1987; Bonin, 2007). Although it is possible to generate syenitic magma by partial melting of a metasomatized mantle (Sutcliffe et al., 1990; Lynch et al., 1993), the more plausible mechanism is by partial melting or fractional crystallization of an alkali rich basalt (Thorpe and Tindle, 1992; Brown and Becker, 1986). Synthetic models assuming mixing of mantle-derived basic and crustal silicic magmas followed by differentiation of hybrid monzonitic melts (Barker et al., 1975; Wickham et al., 1995; Sheppard, 1995; Zhao et al., 1995) require a considerable proportion of the basalt end-member, up to 75 wt.% (Litvinovsky et al., 1999). Formation of syenite by partial melting of the ancient continental crust rocks at high pressures (>15–20 kbar), as it was suggested by Huang and Wyllie (1975, 1981), was not corroborated by melting experiments at 15 to 25 kbar (Litvinovsky et al., 2000). The latter work demonstrated that partial melting of charnockitic gneiss under these conditions leads to formation of granitic rather than syenitic melts even at fairly low degree of melting (<30%). This is caused by crystallization of low-silica garnet + clinopyroxene mineral assemblage in restite, so that partial melt is always enriched in SiO<sub>2</sub>.

In the MTB, the generation of syenite from an enriched mantle-derived source is supported by the similar  $\epsilon\text{Nd}(T)$  and  $I(\text{Sr})$  values in the coeval syenites and basaltic rocks. It was stressed earlier that syenites in the AFS and PA suites are always Qtz-bearing and proportion of quartz increases from 3–8% in earlier intrusive phases to 12–15% in late syenite phases. This is also reflected by the increase SiO<sub>2</sub> from 62–64 wt.% to 66–68 wt.% (see Tables 2S and 4S in

Supplementary Data). For the Bryansky Complex (Figs. 2 and 3), we have shown that the syenite and granite compositions form a quasi-continuous liquid line of decent (Litvinovsky et al., 2002a). A mass-balance calculation revealed that the PA granite could be produced by fractional crystallization of a peralkaline quartz syenite melt with separation of alkali feldspar and subordinate amounts of amphibole and Fe–Ti oxide. This conclusion is consistent with the indistinguishable U–Pb zircon ages (Table 1), Sr–Nd isotopic characteristics (Table 3; Fig. 9) and  $\delta^{18}\text{O}$  values for the syenites and granites from the same suite (Wickham et al., 1996). All these data suggest that highly alkaline syenites and granites from the MTB can be considered as cogenetic, and in some specific cases syenite magmas could be parental to granite.

The fact that PA and AFS granites frequently make up single plutons (e.g. Fig. 3) favors the idea of consanguinity of the two rock types. Their close genetic link has also been noticed in other regions of the CAOB (Leontyev et al., 1981; Wu et al., 2002) and in orogenic belts in Europe (Bowden, 1974; Bonin, 2007), although in some localities, i.e. in southern Australia (Kemp et al., 2005), these rock types are not related.

### 5.2.3. Evidence from the melt inclusion study

The melt inclusion study shows that the liquidus temperature ( $T_L$ ) for the PA syenite exceeds 930–940 °C, and for the PA granite, 760–790 °C (Table 4). On the other hand, melt inclusions in quartz phenocrysts from the comendites are homogenized in a broad temperature interval, from 750 °C to 1100 °C. The difference in liquidus temperature between the granite and syenite can be accounted for by the higher F content (up to 1.6 wt.%) and possibly water in the granite magma. The very high liquidus temperature determined for the comendite requires a more detailed discussion to be presented below.

Although A-type granite magmas could be produced in a wide range of depths (Collins et al., 1982; Clemens et al., 1986; Patiño Douce, 1997; Bonin, 2007), the huge volumes and mantle-like isotope characteristics of the highly alkaline granitoids from the MTB, as well as the enhanced liquidus temperature of silicic magmas suggest that these magmas were generated at great depths. The enhanced pressure at the level of magma generation caused displacement of the eutectic composition to the Ab–Or side of the Ab–Qtz–Or ternary diagram and defined crystallization of quartz as a liquidus phase in granitic melts (Tuttle and Bowen, 1958; Johannes and Holtz, 1996). However, it is unlikely that the early quartz crystals could persist in plutonic rocks during emplacement and slow equilibrium crystallization. Therefore, the  $T_L$  data for plutonic rocks obtained from the melt inclusion study characterize the temperature regime at the level of pluton emplacement, but not the temperature of magma generation in the source region.

In contrast, the early crystals of extrusive rocks may be preserved owing to the rapid ascent and solidification of magma. As the extrusive magma ascends, its crystallization continues; therefore quartz phenocrysts formed at different depths and temperatures may be present in the same sample. This is why only those melt inclusions in phenocryst cores that have the highest temperature of homogenization can be considered to evaluate the magma generation temperature.

The highest  $T_{\text{hom}}$  determined in the quartz phenocryst cores from the comendite samples suggest that the temperature of the generation of the peralkaline silicic magma was about 1100 °C (Table 4). Similar temperatures, up to 1030 °C, were obtained in the melt inclusions trapped in quartz phenocrysts from the porphyritic aegirine granite of the subvolcanic Orot intrusive body in central Transbaikalia (Reyf, 2008). In fact, the data of such a high temperature for A-type silicic magmas are not unique. In quartz phenocrysts from pantellerite from the Pantelleria Island the  $T_{\text{hom}}$  values were reported to reach 1135 °C (Kovalenko et al., 1994). Comparable temperatures in the range of 950–1050 °C were obtained for A-type charnockite intrusions (Bonin, 2007).

Experimental studies indicate that if the liquidus temperature of haplogranitic magma amounts to 1000–1100 °C, and the magma contains about 1–3 wt.% H<sub>2</sub>O, it would require a pressure of 10–15 kbar

**Table 5**  
Summary of the age and Nd isotope data for the Late Paleozoic and Mesozoic PA and AFS granites from the CAOAB.

Pluton, locality	Rock	Age (Ma)		$\epsilon_{\text{Nd}}(T)$		$T_{\text{DM}}^{-2}$ (Ma)	Reference
		Rb–Sr	U–Pb	min	max		
<i>Zhangguangcai Belt (3)</i>							
1	Qingshui		196 ± 4	–2.1	–0.3	1002–1139	Wu et al., 2002
2	Milim		197 ± 2				Wu et al., 2002
3	Maojiatun		213 ± 2	–1.4	+0.3	969–1103	Wu et al., 2002
4	Dawangzhezii	229 ± 12			+3.1	752	Wu et al., 2002
5	Tianguaogang		190 ± 2		+2.3	781	Wu et al., 2002
6	Baishilazi		123 ± 3		+2.0	752	Wu et al., 2002
<i>Great Xing'an Belt (2)</i>							
7	Shaugmachang		106 ± 2	+0.1	+0.2	887–899	Wu et al., 2002
8	Daheishan		292 ± 4	+4.2	+5.3	625–660	Wu et al., 2002
9	Guguhe		264 ± 5		+2.0	872	Wu et al., 2002
10	Songmushan		260 ± 3		+2.1	858	Wu et al., 2002
11	Sizhanlinchang		282 ± 4				Wu et al., 2002
12	Xiaoshantun		285 ± 2		+2.6	835	Wu et al., 2002
13	Nianzishan	125		+2.6	+2.9	683–727	Li & Yu, 1993
		125		+0.9	+4.3	569–728	Wei et al., 2001
14	Baerzhe	122 ± 5		+1.9	+2.5	711–759	Wang & Zhao, 1997
<i>Gobi–Tien Shan Belt (8)</i>							
15	Zhanawula	277 ± 3		+2.6	+6.2	490–744	Hong et al., 1994; 2004
16	Zuhendeleng	284 ± 2		+1.2	+6.5	520–1000	Hong et al., 1994; 2004
17	Baiynula	286 ± 3		+3.6	+5.7	520–701	Hong et al., 1994; 2004
18	Xilinhot		276 ± 2				Shi et al., 2004
19	Khan-Bogd	287 ± 3	290 ± 1				Yarmolyuk et al., 2008
20	Ridge Tost, dyke		318 ± 1		+6.5		Yarmolyuk et al., 2008
	Bimodal volcanic suite, Ridges Noyon and Tost			+4.4	+6.7		Yarmolyuk et al., 2008
				+5.5	+7.4		Yarmolyuk et al., 2008
21	Karamay, W. Junggar	280		+5.0	+5.8		Hong et al., 2004
<i>Gobi–Altai (5) and Main Mongolian Lineament (6) Belts</i>							
22	Dashibalbar association	195.9 ± 3.9		+1.1	+1.5	870–910	Yarmolyuk et al., 2002
				–1.1	–1.6		Yarmolyuk et al., 2002
		188.7 ± 2.8 <sup>a</sup>					Yarmolyuk et al., 2002
23	Bayan-Ulan	221 <sup>a</sup>					Yarmolyuk et al., 2002
24	Mandakh		292 ± 1				Yarmolyuk et al., 2008
25	Tszarta-Khuduk	206					Yarmolyuk et al., 2002
				+0.8	+1.7		
				+0.1	–1.0	990–1030	
26	Bayan–Tsagan range		275 ± 5				Yarmolyuk et al., 2005
27	Boom		294 ± 5				Yarmolyuk et al., 2008
<i>Junggar–Eastern Kazakhstan Belt (7)</i>							
28	Kamste	294 ± 4		+5.2	+7.1	480–620	Chen & Jahn, 2004
	Sawudegeer	303 ± 26		+5.6	+6.5	501–702	Han et al., 1997
	Saertielieke	290 ± 27		+5.1	+5.6	692–1003	Han et al., 1997
	Jierdekala	304 ± 32		+6.1	+6.7	523–557	Han et al., 1997
	South-Tasigake	308 ± 14		+5.1	+5.5	570–878	Han et al., 1997

Numbers of belts and plutons as in Fig. 1.

<sup>a</sup> = <sup>39</sup>Ar/<sup>40</sup>Ar data in amphibole.

for its generation (Stern et al., 1975; Huang and Wyllie, 1975; Johannes and Holtz, 1996; Holtz et al., 2001). When the fluid phase contains also CO<sub>2</sub>, the pressure would be even higher (Keppler, 1989). Temperatures of about 1000–1100 °C are probably the highest yet recorded in the continental crust (Kilpatrick and Ellis, 1992; Rudnick, 1992; Downes, 1993; Del Lama et al., 2000). They exceed significantly the commonly known granulite facies temperatures in the lower crust, with the exception of UHT granulites. Consequently, the high-temperature A-type granite magmas could be produced either in the lower continental crust or in the uppermost subcontinental lithospheric mantle.

### 5.3. Character of the mantle source in the MTB and other belts of the CAOAB

Fig. 10 shows the Nd–Sr isotopic compositions of the highly alkaline granitoids and coeval mafic rocks from the MTB. The four mantle components of Zindler and Hart (1986) are also shown for

reference. Note that precise initial Sr isotopic compositions for high-alkaline rocks due to the generally high Rb/Sr ratios in these rocks are difficult to obtain (see Section 4.2). However, the range and temporal variation of Nd isotopic compositions from stage 1 to 2 to 3 are probably real (Fig. 10A and B). Fig. 10A shows that the mafic rocks (solid symbols) could not be derived from the depleted asthenosphere (DM), nor from a HIMU reservoir alone. The quasi-linear array of mafic rock data seems to suggest that the mantle source regions of the MTB are mixtures of DM and two enriched components (EM-I and EM-II), but with a more important role of EM-I.

The possible sources of silicic magmas are constrained by the following conditions: (1) the isotope compositions of the highly alkaline granitoids and contemporaneous mafic rocks are similar (Table 3; Figs. 9 & 10); (2) lack of evidence for a significant contribution of crust-derived metamorphic component to the generation of the AFS and PA magmas; (3) the related volcanic suites are bimodal,

commonly trachydolerite–rhyolite (comendite); and (4) the plutonic suites are also bimodal, but the proportion of mafic rocks is very small.

It follows from the above constraints that the alkali-rich basic magma could be considered as parental to the highly alkaline silicic magmas. However, the bimodal character of the igneous suites (i.e., absence or rare occurrence of rocks of intermediate composition) suggests that partial melting, rather than fractional crystallization, of gabbroic magma could lead to the generation of silicic melts. The production of highly alkaline granite magma by partial melting of alkali rich basalt was demonstrated in the melting experiments of Sisson et al. (2005). One of the three studied basalt samples (AD19-93) is fairly similar to the mafic rocks under consideration, and in particular, in SiO<sub>2</sub> (50.74%), TiO<sub>2</sub> (1.25%), MgO (4.52%), Na<sub>2</sub>O (3.76%), and K<sub>2</sub>O (2.32%) (cf. with data in Table 2). Partial melting of this sample at 700 MPa to an extent of ~20% produced a granite melt with 3.2 to 3.5 wt.% Na<sub>2</sub>O and 4.7 to 5.94 wt.% K<sub>2</sub>O. Thus, the experimental results show that partial melting of alkali rich basalt/gabbro in the middle crust could produce significant amount of A-type granite magma that can be easily separated and emplaced at shallow levels. The melting experiments also showed that when the extent of melting is increased from 22 to 29%, the SiO<sub>2</sub> content in the melt decreases from 68 to 62 wt.%. Though the proportion of alkalis does not increase (Sisson et al., 2005, Tables 2 and 3), the residual mineral assemblage is enriched in amphibole (20–25%) and biotite (10–15%). Consequently, we may assume that partial melting at a greater depth, where residual mafic minerals are mostly pyroxene and garnet, would result in enriching alkalis in the melt, so that compositions of partial melts would vary from granite to quartz bearing syenite with variable alkali contents, depending upon the degree of melting. The temperature data of 1000–1100 °C for the silicic melts suggest that the partial melting occurred at temperature exceeding  $T_s$  of basalt; therefore, the assumption of 20–30% melting of K-rich mafic rocks in the lower crust looks realistic. Thus, the most plausible ‘mantle’ source of the AFS and PA granitoids is alkali-rich basalt that underplated the lower crust. Soon after the solidification of the basaltic liquid (in the granulite facies P–T condition), it was subjected to partial melting by successive intrusion and underplating of similar magmas.

The Nd-isotopic character of source regions within the CAOB could be correlated with the tectonic setting. Fig. 10B shows all the available data for the magmatic belts of the CAOB. In the Late Paleozoic, the highly alkaline granitoids from the Great Xing'an (field #2 in Fig. 10B), Eastern Kazakhstan (#7) and Gobi–Tien Shan (#8) belts were formed in the continental margin still at the subduction stage, so the  $\epsilon\text{Nd}(T)$  values in granitoids were characterized by more depleted mantle values from +2 to +6. However, negative values prevail in the Early Permian felsic and mafic rocks from the MTB, which were emplaced in intra-continental settings.

In the Early Mesozoic the Nd isotope characteristics of highly alkaline granites from the MTB and the Main Mongolian Lineament (#5) and the Zhangguangcai belt (#3) are quite similar (Fig. 10B). The similarity might be accounted for by the fact that the emplacement of these rocks in all three belts took place soon after the accretion of terranes to the Siberian craton. The tectonic setting was post-accretion intra-continental for all the three belts.

In the Early Cretaceous, peralkaline granites from the Zhangguangcai (#3) and Great Xing'an (#2) belts were produced from a more depleted mantle source during the westward subduction of the Paleo-Pacific plate, hence showing positive  $\epsilon\text{Nd}(T)$  values in highly alkaline granites. In the MTB the Late Mesozoic granitoids were emplaced in a typical intra-continental setting. Consequently, involvement of the EM-I component from the thinned lithosphere mantle produced the slightly negative  $\epsilon\text{Nd}(T)$  values of the felsic and mafic rocks.

## 6. Conclusions

The CAOB is one of the world's most celebrated examples of the widespread distribution of Phanerozoic granitoids. The Late Paleozoic and Mesozoic PA and AFS granitoids and related bimodal volcanic suites form a

network of gigantic belts occupying an area of about 6000 by 2000 km. This network is controlled structurally by the Central Asian Rift System. The present study of the PA and AFS granitoids from the Mongolian–Transbaikalian belt (MTB) leads to the following conclusions:

1. A compilation of age data revealed three stages of granitoid emplacement in the MTB: 285–270 Ma, 230–210 Ma and 150–120 Ma. The plutons of different stages are spatially associated. The same stages of highly alkaline granitoid magmatism are also recognized in other parts of the CAOB, particularly in NE China, Mongolia and Eastern Kazakhstan.
2. The PA and AFS granitoids of different stages have very similar chemical compositions, but their Nd isotope characteristics can be distinguished. The granitoids of stages 1 and 3 have slightly negative  $\epsilon\text{Nd}(T)$  values (–1 to –5), whereas those of stage 2 have near-zero to slightly positive values (0 to +4).
3. Several lines of evidence suggest that the MTB granitoids were produced from enriched mantle-derived sources. They include: (1) Felsic and mafic rocks formed in the same stage have similar  $\epsilon\text{Nd}(T)$  and  $I(\text{Sr})$  values and similar model ages ( $T_{\text{DM}}$ ). (2) the Nd isotopic compositions of the granitoids of each stage vary within a narrow range and do not correlate with the nature and age of the surrounding crustal blocks. (3) The abundant syenites are considered to be cogenetic or, in some cases, parental to the granites. Since experimental and isotope data suggest the derivation of syenite from an enriched mantle source, the related granites (and comendites) can also be regarded as mantle-derived.
4. In the MTB the most probable process for the generation of the highly alkaline granite–quartz syenite magmas is by partial melting (20–30%) of K-rich mafic rocks, which were derived from the lithospheric mantle and underplated the lower crust.
5. An important implication is that the MTB granitoids are mostly juvenile, even if they are not characterized by positive to highly positive  $\epsilon\text{Nd}(T)$  values. This is distinct from the cases in other parts of CAOB (Jahn, 2004) and the Arabian Nubian Shield (Stern, 2002).
6. Although the highly alkaline granite magmas were generated throughout the CAOB during three stages, the tectonic settings at each stage were distinct in different parts of the CAOB, from a rift at an active continental margin to a rift in the interior of an amalgamated continent.

## Acknowledgements

The authors are deeply grateful to V. Yarmolyuk, R. Zeltman and E. Sklyarov for the fruitful discussion and assistance in the compilation of the literary data. Mr. Fu-Lung Lin (IES, Academia Sinica) ably performed geochemical and Sr–Nd isotopic analyses reported herein. Prof. Sun-Lin Chung made available the facility of ICP-MS at National Taiwan University (NTU). The XRF analyses were achieved with the able assistance of Dr. C.Y. Lee, Mlle C.H. Chiu (NTU), and Wen-yu Hsu (IES, Academia Sinica). Greg Shellnutt read an earlier version and provided suggestions for improvement. We are much grateful for the constructive reviews of J.D. Clemens, Fuyuan Wu and Tapani Rämö, and the editorial assistance and comments of Nelson Eby. Bor-ming Jahn acknowledges financial support of the National Science Council (Taiwan) through grants NSC96-2923-M-001-001-MY3, NSC96-2116-M-001-004; NSC97-2752-M-002-003-PAE, NSC97-2116-M-001-011. The investigations in Transbaikalia were supported by the Russian Foundation of Base Researches through grants 93-05-14020, 96-05-64027, 99-05-65138 (to Boris Litvinovsky). Boris Litvinovsky also acknowledges the financial support from the NSC (Taiwan) for a three-month visit to IES in Taipei.

## Appendix A. Supplementary data

Supplementary data associated with this article can be found, in the online version, at doi:10.1016/j.lithos.2009.06.015.

## References

- Barker, F., Wones, D.R., Sharp, W.N., Desborough, G.A., 1975. The Pikes Peak batholith, Colorado Front Range, and a model for the origin of the gabbro-anorthosite-syenite–potassic granite suite. *Precambrian Research* 2, 97–160.
- Bonin, B., 2004. Do coeval mafic and felsic magmas in post-collisional to within-plate regimes necessarily imply two contrasting, mantle and crustal, sources? A review. *Lithos* 78, 1–24.
- Bonin, B., 2007. A-type granites and related rocks: evolution of a concept, problems and prospects. *Lithos* 97, 1–29.
- Bowden, P., 1974. Oversaturated alkaline rocks: granites, pantellerites and comendites. In: Sorensen, H. (Ed.), *The Alkaline Rocks*. John Wiley and Sons, London–New York, A Wiley–Interscience Publication, pp. 109–123.
- Brown, P.E., Becker, S.M., 1986. Fractionation, hybridization and magma mixing in the Kialineq center East Greenland. *Contribution to Mineralogy and Petrology* 92, 57–70.
- Buslov, M.M., Fujiwara, Y., Imata, K., Semakov, N.N., 2004. Late Paleozoic–Early Mesozoic geodynamics in Central Asia. *Gondwana Research* 7, 791–808.
- Chen, B., Jahn, B.M., 2004. Genesis of post-collisional granitoids and basement nature of the Junggar Terrane, NW China: Nd–Sr isotope and trace element evidence. *Journal of Asian Earth Sciences* 23, 691–704.
- Chen, B., Jahn, B.M., Tian, W., 2009. Evolution of the Solonker suture zone: constraints from zircon U–Pb ages, Hf isotopic ratios and whole-rock Nd–Sr isotope compositions of subduction- and collision-related magmas and forearc sediments. *Journal of Asian Earth Sciences* 34, 245–257.
- Clemens, J.D., Holloway, J.R., White, A.J.R., 1986. Origin of an A-type granite: experimental constraints. *American Mineralogist* 71, 317–324.
- Collins, W.J., Beams, S.D., White, A.J.R., Chappell, B.W., 1982. Nature and origin of A-type granites with particular reference to Southeastern Australia. *Contribution to Mineralogy and Petrology* 80, 189–200.
- Del Lama, E.A., Zanardo, A., Oliveira, M.A.F., Morales, N., 2000. Exhumation of high-pressure granulites of the Guaxup Complex, Southeastern Brazil. *Geological Journal* 35, 231–249.
- DePaolo, D.J., Linn, A.M., Schubert, G., 1991. The continental crustal age distribution: methods of determining mantle separation ages from Sm–Nd isotopic data and application to the southwestern United States. *Journal of Geophysical Research* 96, 2071–2088.
- Donskaya, T.V., Windley, B.F., Mazukabzov, A.M., Kroener, A., Sklyarov, E.V., Gladkochub, D.P., Ponomarchuk, V.A., Badarch, G., Reichow, M., 2008. Age and evolution of Mesozoic metamorphic core complexes in southern Siberia and northern Mongolia. *Journal of the Geological Society* 165, 405–421.
- Downes, H., 1993. The nature of the lower continental crust of Europe: petrological and geochemical evidence from xenoliths. *Physics of the Earth and Planetary Interiors* 79, 195–218.
- Eby, G.N., 1992. Chemical subdivision of the A-type granitoids: petrogenetic and tectonic implications. *Geology* 20, 641–644.
- Han, B.F., Wang, S.G., Jahn, B.M., Hong, D.W., Kagami, H., Sun, Y.L., 1997. Depleted-mantle magma source for the Ulungur River A-type granites from north Xinjiang, China: Geochemistry and Nd–Sr isotopic evidence, and implication for Phanerozoic crustal growth. *Chemical Geology* 138, 135–159.
- Heinhorst, J., Lehmann, B., Ermolov, P., Serykh, V., Zhuratina, S., 2000. Paleozoic crustal growth and metallogeny of central Asia: evidence from magmatic–hydrothermal ore systems of central Kazakhstan. *Tectonophysics* 328, 69–87.
- Holtz, F., Johannes, W., Tamic, N., Behrens, H., 2001. Maximum and minimum water contents of granitic melts generated in the crust: a reevaluation and implications. *Lithos* 56, 1–14.
- Hong, D.W., Chang, W.J., Huang, H.Z., Xiao, Y.J., Xu, H.M., Jin, M.Y., 1994. The Permian alkaline granites in Central Inner Mongolia and their geodynamic significance. *Journal of SE Asian Earth Sciences* 10, 169–176.
- Hong, D.W., Wang, S.G., Han, B.F., Jin, M.Y., 1996. Post-orogenic alkaline granites from China and comparisons with anorogenic alkaline granites elsewhere. *Journal of SE Asian Earth Sciences* 13, 13–27.
- Hong, D.W., Zhang, J.S., Wang, T., Wang, S.G., Xie, X.L., 2004. Continental crustal growth and the supercontinental cycle: evidence from the Central Asian orogenic belt. *Journal of Asian Earth Sciences* 23, 799–813.
- Huang, W.L., Wyllie, P.J., 1975. Melting reactions in the system NaAlSi<sub>3</sub>O<sub>8</sub>–SiO<sub>2</sub> to 35 kilobar, dry and with excess water. *Journal of Geology* 83, 737–748.
- Huang, W.L., Wyllie, P.J., 1981. Phase relationship of S-type granite with H<sub>2</sub>O to 35 kbar: muscovite granite from Harney Peak, South Dakota. *Journal of Geophysical Research* 86, 10515–10529.
- Jahn, B.-M., 2004. The Central Asian Orogenic Belt and growth of the continental crust in the Phanerozoic. Geological Society of London, Special Publications 226, 73–100.
- Jahn, B.M., Wu, F.Y., Chen, B., 2000. Granitoids of the Central Asian Orogenic Belt and continental growth in the Phanerozoic. *Transactions of Royal Society, Edinburgh, Earth Sciences* 91, 181–193.
- Jahn, B.M., Wu, F.Y., Capdevila, R., Martineau, F., Wang, Y.X., Zhao, Z.H., 2001. Highly evolved juvenile granites with tetrad REE patterns: the Woduhe and Baerzhe granites from the Great Xing'an (Khangai) Mountains in NE China. *Lithos* 59, 171–198.
- Jahn, B.-M., Capdevila, R., Liu, D., Vernov, A., Badarch, G., 2004. Sources of Phanerozoic granitoids in the transect Bayanhongor–Ulan Baator, Mongolia: geochemical and Nd isotopic evidence, and implications of Phanerozoic crustal growth. *Journal of Asian Earth Sciences* 23, 629–653.
- Johannes, W., Holtz, F., 1996. Petrogenesis and experimental petrology of granitic rocks. Springer-Verlag, Berlin. 330 pp.
- Kemp, A.I.C., Wormald, R.J., Whitehouse, M.J., Price, R.C., 2005. Hf isotopes in zircon reveal contrasting sources and crystallization histories for alkaline to peralkaline granites in Temora, southeastern Australia. *Geology* 33, 797–800.
- Kepler, H., 1989. The influence of the fluid phase composition on the solidus temperatures in the haplogranite system NaAlSi<sub>3</sub>O<sub>8</sub>–KAlSi<sub>3</sub>O<sub>8</sub>–SiO<sub>2</sub>–H<sub>2</sub>O–CO<sub>2</sub>. *Contribution to Mineralogy and Petrology* 102, 321–327.
- Keto, L.S., Jacobsen, S.B., 1987. Nd and Sm isotope variations of Early Paleozoic oceans. *Earth and Planetary Scientific Letter* 84, 27–41.
- Khain, E.V., Bibikova, E.V., Kroner, A., Zhuravlev, D.Z., Sklyarov, E.V., Fedotova, A.A., Kravchenko-Berezhnoy, I.R., 2002. The most ancient ophiolite in the Central Asian fold belt: U–Pb and Pb–Pb evidence from the Dunzhugur Complex, Eastern Sayan, Siberia, and geodynamic implications. *Earth and Planetary Science Letters* 199, 311–325.
- Khanchuk, A.N., Mikhailov, V., 1989. Geodynamic evolution of southern Far East in the Middle Paleozoic–Early Mesozoic. Pacific margin of Asia. *Geology (in Russian)*. Nauka, Moscow, pp. 215–255.
- Kilpatrick, J.A., Ellis, D.J., 1992. C-type magmas: igneous charnockites and their extrusive equivalents. *Transaction of the Royal Society of Edinburgh, Earth Sciences* 83, 155–164.
- Kovalenko, V.I., Naumov, V.B., Solovova, I.P., Girmis, A.V., Hervig, R.L., Boriani, A., 1994. Volatiles, composition and conditions of crystallization of magmas formed basalt–pantellerite association at Pantelleria Island (by study of melt and fluid inclusions). *Petrologia* 2, 24–42 (in Russian).
- Kovalenko, V.I., Yarmolyuk, V.V., Kovach, V.P., Kotov, A.B., Kozlovsky, A.M., Salmnikova, E.B., Larin, A.M., 2004. Isotope provinces, mechanisms of generation and sources of the continental crust in the Central Asian Mobile Belt: geological and isotopic evidence. *Journal of Asian Earth Sciences* 23, 605–627.
- Kuzmin, D.V., Chupin, V.P., Litvinovsky, B.A., 1999. Temperature and composition of magmas formed trachybasalt–comendite suite in the Tsagan-Khurtei Range, West Transbaikalia (by melt inclusions study). *Russian Geology and Geophysics* 40, 62–72.
- Leontyev, A.N., Litvinovsky, B.A., Gavrilo, S.P., Zakharov, A.A., 1981. Paleozoic granitoid magmatism of the Central-Asian fold belt (in Russian). *Nauka, Novosibirsk*. 330 pp.
- Li, P.Z., Yu, J.S., 1993. Nianzishan miarolitic alkaline granite stock, Heilongjiang — its ages and geological implications (in Chinese with English abstract). *Geochimica* 4, 389–398.
- Liégeois, J.P., Navez, J., Hertogen, J., Black, R., 1998. Contrasting origin of post-collisional high-K calc-alkaline and shoshonitic versus alkaline and peralkaline granitoids. The use of sliding normalization. *Lithos* 45, 1–28.
- Litvinovsky, B.A., Posokhov, V.F., Zanzvilevich, A.N., 1995a. Unusual Rb–Sr data on the age of two typical peralkaline granitoid plutons in Western Transbaikalia. *Russian Geology and Geophysics* 36, 65–72.
- Litvinovsky, B.A., Zanzvilevich, A.N., Kalmanovich, M.A., 1995b. Recurrent mixing and mingling of coexisting syenite and basalt magmas in the Ust-Khilok massif, Transbaikalia, and its petrologic significance. *Petrology* 2, 115–137.
- Litvinovsky, B.A., Zanzvilevich, A.N., Wickham, S.M., Steele, I.M., 1999. Origin of syenite magmas in A-type granitoid series: syenite–granite series from Transbaikalia. *Petrology* 7, 483–508.
- Litvinovsky, B.A., Steel, I.M., Wickham, S.M., 2000. Silicic magma formation in over-thickened crust: melting of charnockite and leucogranite at 15, 20 and 25 kbar. *Journal of Petrology* 41, 717–737.
- Litvinovsky, B.A., Yarmolyuk, V.V., Vorontsov, A.A., Zhuravlev, D.Z., Posokhov, B.F., Sandimirova, G.P., Kuzmin, D.V., 2001. Late Triassic stage of formation of the Mongolian–Transbaikalian alkaline–granitoid province: data of isotope–geochemical studies. *Russian Geology and Geophysics* 42, 445–455.
- Litvinovsky, B.A., Jahn, B.-M., Zanzvilevich, A.N., Saunders, A., Poulsen, S., 2002a. Petrogenesis of syenite–granite suites from the Bryansky Complex (Transbaikalia, Russia): implications for the origin of A-type granitoid magmas. *Chemical Geology* 189, 105–133.
- Litvinovsky, B.A., Jahn, B.M., Zanzvilevich, A.N., Shadaev, M.G., 2002b. Crystal fractionation in the petrogenesis of an alkali monzodiorite–syenite series: the Oshurkovo plutonic sheeted complex, Transbaikalia, Russia. *Lithos* 64, 97–130.
- Loiselle, M.C., Wones, D.R., 1979. Characteristics and origin of anorogenic granites. *Geological Society of America Abstract Programs* 11, 468.
- Lykhin, D.A., Kostitsyn, Yu.A., Kovalenko, V.I., Yarmolyuk, V.V., Salmnikova, E.B., Kotov, A.B., Kovach, V.P., Ripp, G.S., 2001. Ore-bearing magmatism in the Yermakovka berillium deposit in the western Transbaikalia: age, magma sources and interrelations with ore-forming processes. *Geology of the Ore Deposits* 43, 52–70.
- Lynch, D.J., Musselman, T.E., Gutmann, J.T., Patchet, P.J., 1993. Isotopic evidence for the origin of Cenozoic volcanic rocks in the Pinacate volcanic field, northwestern Mexico. *Lithos* 29, 295–302.
- Mossakovsky, A.A., Ruzhentsev, S.V., Samygin, S.G., Kheraskova, T.N., 1994. Central Asian fold belt: geodynamic evolution and formation history. *Geotectonics* 27, 445–474.
- Parfenov, L.M., Berzin, N.A., Khanchuk, A.I., Bagarov, G., Belichenko, V.G., Bulgatov, A.N., Dril, S.I., Kirillova, G.L., Kuzmin, M.I., Nokleberg, W.J., Prokopyev, A.V., Timofeev, V.F., Tomurtogoo, O., Yang, H., 2003. A model of the formation of orogenic belts in Central and Northeast Asia. *Geology of the Pacific Ocean* 22, 7–41.
- Patiño Douce, A.E., 1997. Generation of metaluminous A-type granites by low-pressure melting of calc-alkaline granitoids. *Geology* 25, 743–746.
- Posokhov, B.F., Shadaev, M.G., Litvinovsky, B.A., Zanzvilevich, A.N., Khubanov, V.B., 2005. Rb–Sr age and sequence of formation of granitoids in the Khorinsk volcano–plutonic structure in the Mongolian–Transbaikalian Belt. *Russian Geology and Geophysics* 46, 625–632.
- Reichow, M.K., Saunders, A.D., White, R.V., Parrish, R.R., Litvinovsky, B., Zanzvilevich, A.N., 2003. Silicic magmatism in Transbaikalia, Russia, and its link with the Siberian Traps. *Geophysical Research, Abstracts Volume 5*, 05048.
- Reyf, F.G., 1997. Direct evolution of W-rich brines from crystallizing melt within the Mariktikan granite pluton, west Transbaikalia. *Mineral Deposita* 32, 475–490.
- Reyf, F.G., 2004. Immiscible phases of magmatic fluid and their relation to Be and Mo mineralization at the Yermakovka F–Be deposit, Transbaikalia, Russia. *Chemical Geology* 210, 49–71.
- Reyf, F.G., 2008. Peralkaline granites and berillium (phenakite–bertrandite) ore mineralization in the Orot and Yermakovka deposits. *Geochemistry International* 3, 1–21.
- Roedder, E., 1979. Origin and significance of melt inclusions. *Bulletin de Mineralogie* 102, 487–510.

- Rudnick, R.L., 1992. Xenoliths – Samples of the lower continental crust. In: Fountain, D.M., Arculus, R.J., Kay, R.W. (Eds.), *the lower continental crust*. Elsevier, New York, pp. 269–316.
- Sengör, A.M.C., Natal'in, B.A., 1996. Turkin-type orogeny and its role in making of continental crust. *Annual Review of Earth and Planetary Sciences* 24, 263–337.
- Sengör, A.M.C., Natal'in, B.A., Burtman, V.S., 1993. Evolution of Altaid tectonic collage and Paleozoic crustal growth in Eurasia. *Nature* 364, 299–307.
- Sheppard, S., 1995. Hybridization of shoshonitic lamprophyre and calc-alkaline granite magma in the Early Proterozoic Mt. Bandey igneous suite, Northern Territory. *Australian Journal of Earth Sciences* 42, 173–185.
- Shi, Y.R., Liu, D.Y., Zhang, Q., Jian, P., Zhang, F.Q., Miao, L.C., Shi, G.H., Zhang, L.Q., Tao, H., 2004. SHRIMP dating of diorites and granites in southern Sonidzuqi, Inner Mongolia. *Acta Geologica Sinica* 78, 789–799.
- Sisson, T.W., Ratajevski, K., Hankins, W.B., Glazner, A.F., 2005. Voluminous granitic magmas from common basaltic source. *Contributions to Mineralogy and Petrology* 148, 635–661.
- Sklyarov, Ye.V., Mazukabzov, A.M., Donskaya, T.A., Doronina, N.A., Shafeyev, A.A., 1994. Metamorphic core complex in the Zagan Range, Transbaikalia (in Russian). *Transactions (Doklady) Academia Nauk (Russian Academy of Sciences)* 339, 83–86.
- Stern, R.J., 2002. Crustal evolution in the East African Orogen: a neodymium isotopic perspective. *Journal of Africa Earth Sciences* 34, 109–117.
- Stern, C.R., Huang, W.L., Wyllie, P., 1975. Basalt-andesite-rhyolite-H<sub>2</sub>O: crystallization intervals with excess H<sub>2</sub>O and H<sub>2</sub>O-undersaturated liquidus surfaces to 35 kilobars, with implications for magma genesis. *Earth and Planetary Science Letters* 28, 189–196.
- Student, J.J., Bodnar, R.J., 1999. Synthetic fluid inclusions XIV: coexisting silicate melt and aqueous fluid inclusions in the haplogranite-H<sub>2</sub>O-NaCl-KCl system. *Journal of Petrology* 10, 1509–1525.
- Stupak, F.M., 1999. New data on geology, age and tectonic of Early Mesozoic volcanic series of Northern Transbaikalia (in Russian). *Doklady Russian Academy of Sciences* 369, 503–506.
- Sun, S.S., McDonough, W.F., 1989. Chemical and isotopic systematics of oceanic basalts: implications for mantle compositions and processes. In: A.D. Saunders and M.J. Norry (Eds.), *Magmatism in the Ocean Basins*. Geological Society Special Publication 42, 313–345.
- Sutcliffe, R.H., Smith, A.R., Doherty, W., Barnett, R.L., 1990. Mantle derivation of Archean amphibole-bearing granitoid and associated mafic rocks: evidence from the southern Superior Province, Canada. *Contribution to Mineralogy and Petrology* 105, 255–274.
- Thomas, R., Klemm, W., 1997. Microthermometry study of silicate melt inclusions in Variscan granites from SE Germany: volatile contents and entrapment conditions. *Journal of Petrology* 38, 1753–1765.
- Thorpe, R.S., Tindle, A.G., 1992. Petrology and petrogenesis of a Tertiary diorite/peralkaline-subalkalinetrachyte-rhyolite dike association from Lundy, Bristol Channel. *Geological Journal* 27, 101–117.
- Tsygankov, A.A., Matukov, D.I., Berezhnaya, N.G., Larionov, A.N., 2007. Late Paleozoic granitoids of western Transbaikalia: magma sources and stages of formation. *Russian Geology and Geophysics* 48, 120–140.
- Tuttle, O.F., Bowen, N.L., 1958. Origin of granite in light of experimental studies in the system NaAlSi<sub>3</sub>O<sub>8</sub>-KAlSi<sub>3</sub>O<sub>8</sub>-SiO<sub>2</sub>-H<sub>2</sub>O. *Geological Society of America Memoir* 74, 153 pp.
- Wang, Y.X., Zhao, Z.H., 1997. Geochemistry and origin of the Baerzhe REE-Nb-Be-Zr superlarge deposit (in Chinese with English abstract). *Geochimica* 26, 24–35.
- Wang, S.G., Han, B.F., Hong, Dawei, Xu, B.L., Sun, Y.Y., 1995. Geochemistry and tectonic significance of alkali granites along the Ulungur River, Xijiang. *Chinese journal of Geochemistry* 14 (4), 323–335.
- Webster, J.D., Rebbert, C.R., 2001. The geochemical signature of fluid-saturated magma determined from silicate melt inclusions in Anson Island granite xenolith. *Geochimica and Cosmochimica Acta* 65, 123–136.
- Wei, C.S., Zheng, Y.F., Zhao, Z.F., 2001. Nd-Sr-O isotopic geochemistry constraints on the age and origin of the A-type granites in eastern China (in Chinese with English abstract). *Acta Petrologica Sinica* 17, 95–111.
- Whalen, J.B., 2005. A-type granites: >25 years later. Abstracts of the 15th Annual V.M. Goldschmidt Conference, Moscow, Idaho, May 2005. *Geochimica and Cosmochimica Acta* 69, A84 Special Supplement.
- Whalen, J.B., Currie, K.L., Chappell, B.W., 1987. A-type granites: geochemical characteristics, discrimination and petrogenesis. *Contribution to Mineralogy and Petrology* 95, 407–419.
- Wickham, S.M., Litvinovsky, B.A., Zanzvilevich, A.N., Bindeman, I.N., Schauble, E.A., 1995. Geochemical evolution of Phanerozoic magmatism in Transbaikalia, East Asia: a key constraint on the origin of K-rich silicic magmas and the process of cratonization. *Journal of Geophysical Research* 100, 15641–15654.
- Wickham, S.M., Albertz, A.D., Zanzvilevich, A.N., Litvinovsky, B.A., Bindeman, I.N., Schauble, E.A., 1996. A stable isotope study of anorogenic magmatism in East Central Asia. *Journal of Petrology* 37, 1063–1095.
- Windley, B.F., Alexeiev, D., Xiao, W.J., Kroner, A., Badarch, G., 2007. Tectonic models for accretion of the Central Asian Orogenic Belt. *Bicentennial Review. Journal of Geological Society* 164, 31–47.
- Wu, F.Y., Jahn, B.M., Wilde, S., Sun, D.Y., 2000. Phanerozoic crustal growth: U-Pb and Sr-Nd isotopic evidence from the granites in northeast China. *Tectonophysics* 328, 89–103.
- Wu, F.Y., Sun, D.Y., Li, H.M., Jahn, B.M., Wilde, S.A., 2002. A-type granites in Northeastern China: age and geochemical constraints on their petrogenesis. *Chemical Geology* 187, 143–171.
- Wu, F.Y., Jahn, B.M., Wilde, S.A., Lo, C.H., Yui, T.F., Lin, Q., Ge, W.C., Sun, D.Y., 2003a. Highly fractionated I-type granites in northeastern China (I): Geochronology and petrogenesis. *Lithos* 66, 241–243.
- Wu, F.Y., Jahn, B.M., Wilde, S.A., Lo, C.H., Yui, T.F., Lin, Q., Ge, W.C., Sun, D.Y., 2003b. Highly fractionated I-type granites in northeastern China (II): isotope geochemistry and implications for crustal growth in the Phanerozoic. *Lithos* 67, 191–204.
- Wu, F.Y., Sun, D.Y., Jahn, B.M., Wilde, S., 2004. A Jurassic garnet-bearing granitic pluton from NE China showing tetrad REE patterns. *Journal of Asian Earth Sciences* 23, 731–744.
- Wu, F.Y., Lin, J.Q., Wilde, S.A., Zhang, X.O., Yang, J.H., 2005. Nature and significance of the early Cretaceous giant igneous event in eastern China. *Earth and Planetary Science Letters* 233, 103–119.
- Wu, F.Y., Zhao, G.C., Sun, D.Y., Wilde, S.A., Yang, J.H., 2007a. The Hulan Group: its role in the evolution of the Central Asian Orogenic Belt of NE China. *Journal of Asian Earth Sciences* 30, 542–556.
- Wu, F.Y., Yang, J.H., Lo, C.H., Wilde, S.A., Sun, D.Y., Jahn, B.M., 2007b. The Heilongjiang Group: a Jurassic accretionary complex in the Jiamusi Massif at the western Pacific margin of northeastern China. *Island Arc* 16, 156–172.
- Xiao, W., Windley, B.F., Hao, J., Zhai, M., 2003. Accretion leading to collision, and the Permian Solonker suture, Inner Mongolia, China: termination of the central Asia Orogenic Belt. *Tectonics* 22, 1069. doi:10.1029/2002TC001484.
- Xiao, W., Windley, B.F., Badarch, G., Sun, S., Li, J., Qin, K., Wang, Z., 2004. Paleozoic accretionary and convergent tectonics of the southern Altai: implication for the growth of Central Asia. *Journal of Geological Society, London* 161, 339–342.
- Yang, J.H., Chung, S.L., Wilde, S.A., Wu, F.Y., Chu, M.F., Lo, C.H., Fan, H.R., 2005. Petrogenesis of post-orogenic syenites in the Sulu Orogenic Belt, East China: geochronological, geochemical and Nd-Sr isotopic evidence. *Chemical Geology* 214, 99–125.
- Yanshin, A.L. (Ed.), 1980. *Tectonics of Northern Eurasia*. Nauka, Moscow. 400 pp. (in Russian).
- Yarmolyuk, V.V., 1983. Late Paleozoic volcanism in the intracratonic paleorifts of Central Asia. *Nauka, USSR, Moscow*. 198 pp. (in Russian).
- Yarmolyuk, V.V., Ivanov, V.G., Kovalenko, V.I., 1998. Sources of the intraplate magmatism of Western Transbaikalia in the late Mesozoic-Cenozoic: trace element and isotope data. *Petrology* 6, 101–124.
- Yarmolyuk, V.V., Litvinovsky, B.A., Kovalenko, V.I., Jahn, B.M., Zanzvilevich, A.N., Vozontsov, A.A., Zhuravlev, D.Z., Posokhov, V.F., Kuzmin, D.V., Sandimirova, G.P., 2001. Formation stages and sources of the peralkaline granitoid magmatism of the Northern Mongolian-Transbaikalia Rift Belt during Permian and Triassic. *Petrology* 9, 302–328.
- Yarmolyuk, V.V., Kovalenko, V.I., Salnikova, E.B., Budnikov, S.V., Kovach, V.P., Kotov, A.B., Ponomarchuk, V.A., 2002. Tectono-magmatic zoning, magma sources, and geodynamic of the Early Mesozoic Mongolo-Transbaikalian magmatic area. *Geotectonics* 36, 293–311.
- Yarmolyuk, V.V., Kovalenko, V.I., Kozlovsky, A.M., Vorontsov, A.A., Savatenkov, V.M., 2005. Late Paleozoic-Early Mesozoic Rift System of Central Asia: composition of magmatic rocks, sources, order of formation and geodynamics. In: Kovalenko, V.I. (Ed.), *Tectonic Problems of Central Asia*. World of Science Publisher, Moscow, pp. 197–226.
- Yarmolyuk, V.V., Kovalenko, V.I., Salnikova, E.B., Kovach, V.P., Kozlovsky, A.M., Kotov, A.B., Ledev, V.I., 2008. Geochronology of magmatic rocks and conditions of formation of Late Paleozoic Southern-Mongolian active margin of the Siberian continent. *Stratigraphy and Geological Correlation* 16, 162–181.
- Yermolov, P.V., Vladimirov, A.G., Tikhomirova, I.I., 1988. Petrology of silica oversaturated apaitic alkaline rocks (in Russian). *Nauka, Novosibirsk*. 86 pp.
- Zanzvilevich, A.N., Litvinovsky, B.A., Andreev, G.V., 1985. The Mongolian-Transbaikalian peralkaline granitoid province (in Russian). *Nauka, Moscow*. 231 pp.
- Zanzvilevich, A.N., Litvinovsky, B.A., Wickham, S.M., Bea, F., 1995. Genesis of alkaline and peralkaline syenite-granite series: the Kharitonovo pluton (Transbaikalia, Russia). *Journal of Geology* 103, 127–145.
- Zhang, J.H., Ge, W.C., Wu, F.Y., Wilde, S.A., Yang, J.H., Liu, X.M., 2008. Large-scale early Cretaceous volcanic events in the northern Great Xing'an Range, Northeastern China. *Lithos* 102, 138–157.
- Zhao, J.X., Shiraishi, K., Ellis, D.J., Sheratin, J.W., 1995. Geochemical and isotopic studies of syenites from the Yamato Mountains, East Antarctica: implications of the origin of syenitic magmas. *Geochimica and Cosmochimica Acta* 59, 1363–1382.
- Zindler, A., Hart, S., 1986. Chemical geodynamics. *Annual Review of Earth Planetary Sciences* 14, 493–571.
- Zonenshine, L.P., Kuzmin, M.I., 1993. Deep geodynamics of the Earth. *Russian Geology and Geophysics* 34, 1–9.